CHAIR OF HYDROLOGY
ALBERT- LUDWIGS-UNIVERSITÄT FREIBURG I. BR.

FABIAN FRITZ

SOIL WATER INFILTRATION AND DISTRIBUTION PATTERNS UNDER DIFFERENT FOREST STANDS IN APPLICATION OF STABLE WATER ISOTOPE ANALYISIS

1ST SUPERVISOR: DR. ORLOWSKI
2ND SUPERVISOR: PROF. DR. WERNER

MASTER THESIS
TO OBTAIN THE DEGREE OF MASTER OF SCIENCE
IN HYDROLOGY

FREIBURG I. BR., DECEMBER 2021

Contents

List of Figures

List of Tables

Acknowledgement

First of all, I would like to thank Dr. Natalie Orlowski for the supervision and correction of my Master's Thesis and for her support during the entire process. Furthermore, I want to thank Prof. Dr. Christiane Werner for being the second supervisor of my thesis.
I also want to thank the entire Ecohydrology team for the set up and procedure of our project in Ettenheim. Special thanks go to Judith Mach and Dr. Stefan Seeger for the construction and installation as well as the operation of the in situ probes.
In addition, I would like to thank Dr. Barbara Herbstritt for her comprehensive support and advice in the laboratory and Britta Kattenstroh for her technical support during the installation of the sensors. Further, I want to thank the staff from the Chairs of Plant Physiology and Soil Ecology for the CEC and C/N analysis. Finally, I would like to thank my family and friends for being patient with me during this phase.

Abstract

Forest ecosystems must adapt to changing environmental conditions associated with climate change. This includes changing soil water availability. Infiltration and distribution of water are important processes for understanding the water balance in forest soils and water availability to plants. We investigated water distribution and infiltration patterns using water stable isotopes (^{2}H und ^{18}O) under natural conditions in a 0.75 ha forest study site in the Blackforest, Germany.

Therefore, we analyzed the spatial and temporal variability of the isotopic composition of precipitation, throughfall and soil water in the unsaturated zone. For this purpose, we installed a large number of in situ isotope probes, complemented with several destructive measurements using the equilibrium bag method. Furthermore, we analyzed physiochemical soil properties at our site to evaluate the effect of these properties on the soil water isotopes. Additionally, we used isotope measurements to investigate the influence of European beech (Fagus Sylvatica) and Norway spruce (Picea Abies) on soil water infiltration and distribution patterns. We investigated the differences in the isotopic composition of soil water among pure and mixed stands using analysis of variances and tested the effect of physicochemical soil properties by linear regression.

Our results show high temporal variability of the isotopic composition of precipitation and throughfall and distinctly demonstrate isotopic fractionation of shallow soil water by evaporation. Further, we found significant dependencies on ^{2}H by matric potential ($p < 0.001$) as well as indications of deeper rooting of beech in mixed stands. We conclude that high-resolution isotope measurements with the in situ probes offer many opportunities and point to the potential of holistic interdisciplinary studies between hydrologists, soil ecologists, and plant physiologists.

Zusammenfassung

Waldökosysteme müssen sich aufgrund des Klimawandels an verändernde Umweltbedingungen anpassen. Dazu gehört auch eine sich verändernde Wasserverfügbarkeit. Infiltration und Verteilung von Wasser sind wichtige Prozesse für das Verständnis des Wasserhaushalts in Waldböden und der Wasserverfügbarkeit für Pflanzen. Wir untersuchten Wasserverteilungs- und Infiltrationsmuster mit Hilfe stabiler Wasserisotope (^{2}H und ^{18}O) unter natürlichen Bedingungen in einem 0.75 ha großen Waldgebiet im Schwarzwald, Deutschland.

Dazu analysierten wir die räumliche und zeitliche Variabilität der Isotopenzusammensetzung von Niederschlag und Bodenwasser in der ungesättigten Zone. Zu diesem Zweck installierten wir eine große Anzahl von in-situ-Isotopensonden, ergänzt durch mehrere destruktive Messungen mit der Equilibrier Methode. Außerdem analysierten wir die physiochemischen Bodeneigenschaften an unserem Standort, um den Einfluss dieser Eigenschaften auf die Bodenwasserisotope zu bewerten. Zudem untersuchten wir anhand der Isotopenmessungen den Einfluss von Rotbuche (Fagus Sylvatica) und Fichte (Picea Abies) auf die Infiltration und Verteilung des Bodenwassers. Wir untersuchten die Unterschiede in der Isotopenzusammensetzung des Bodenwassers zwischen Rein- und Mischbeständen mit Varianzanalysen und den Einfluss der physikalisch-chemischen Bodeneigenschaften über lineare Regression.

Unsere Ergebnisse zeigen eine hohe zeitliche Variabilität der Isotopenzusammensetzung von Niederschlag und belegen deutlich die Isotopenfraktionierung von Oberflächen nahen Bodenwasser durch Verdunstung. Darüber hinaus fanden wir signifikante Abhängigkeiten von ^{2}H durch Matrix Potential ($p < 0.001$) sowie Hinweise auf eine tiefere Durchwurzelung der Buche in Mischbeständen. Wir kommen zu dem Schluss, dass hochauflösende Isotopenmessungen mit den in situ Sonden viele Möglichkeiten bieten und verweisen auf das Potenzial ganzheitlicher interdisziplinärer Studien zwischen Hydrologen, Bodenökologen und Pflanzenphysiologen.

1. Introduction

The shape of forest ecosystems depends on the interaction between the atmosphere, plants and soils. Understanding hydrological processes within these systems are fundamental for understanding the complex interrelations behind them and aids in the adaption to environmental changes, especially in the context of climate change.

The application of stable water isotopes (^{2}H and ^{18}O) as natural tracers are effective for hydrological and ecohydrological investigations as proven by various studies. They are used to estimate origin and residence times (Brinkmann et al., 2018; Garvelmann et al., 2012) water transit times and flow paths (Mennekes et al., 2021; Sprenger, Seeger, et al., 2016) and infiltration and mixing of water in the unsaturated zone (Gazis & Feng, 2004; Mueller et al., 2014), showing high spatiotemporal variability of water dynamics both in plants and soils (Dawson & Ehleringer, 1991; Evaristo et al., 2015; Gaj et al., 2016; Goldsmith et al., 2019; Oerter & Bowen, 2017, 2019; Seeger & Weiler, 2021).

The investigation of the quantitative water dynamics in the soil-plant-atmosphere-continuum (SPAC) is possible due to the conservative nature of the water stable isotopes as an integrated component of the water molecule. Water is subjected to multiple, measurable fractionation processes during physicochemical and biological processes and reactions, most importantly the kinetic and the equilibrium fractionation during phase change (Craig, 1961a; Dansgaard, 1964; Friedman, 1953; Kendall & Caldwell, 1998; Majoube, 1971) providing an imprinted isotopic signature of spatially and temporally separated water pools.

1.1 Impact of Soil Properties on Isotopes

Studies have shown high spatiotemporal variability of the isotopic composition in soil waters under natural conditions (Goldsmith et al., 2019; Sprenger et al., 2018; Sprenger, Seeger, et al., 2016), raising questions about the underlying processes that cause this variability.

Evidence is accumulating that the extent of water isotope fractionation in soils may be related to soil physicochemical properties. Studies have found that the matric potential and thus water retention characteristics of soils which are mainly affected by soil texture and organic matter content have an impact on the equilibrium fractionation of soil water (Gaj & McDonnell, 2019; Orlowski & Breuer, 2020). Furthermore, the clay mineralogy, thus the cation exchange capacity (Adams et al., 2020; Gaj et al., 2017; Moreau-Le Golvan et al., 1997; E. Oerter et al., 2014; Savin & Hsieh, 1998; Vandevelde & Bowen, 2013), carbonate content (Meißner et al., 2014) and soil water content (Hendry et al., 2015; Kelln et al., 2001; Meißner et al., 2014; Newberry et al., 2017; Wassenaar et al., 2008) may result in different isotope values of extracted soil water. However, this is mainly related to the applied extraction method for isotope analysis (e.g. cryogenic vacuum extraction).

Furthermore, organic contamination can lead to artifacts of measured ^{2}H and ^{18}O values when measured with laser spectroscopy (Barbeta et al., 2019; Martín-Gómez et al., 2015; Orlowski et al., 2016; Gralher et al., 2016) for soils with a high organic matter content.

In addition, extracting soil water under different suction pressures, obtains water from different water pools or pore spaces (Bowers et al., 2020; Meißner et al., 2014; Orlowski et al., 2016, 2019).

1.2 Soil Water Extraction Methods

For the analysis of the isotopic composition of water in the unsaturated zone multiple methods regarding soil pore water extraction have been developed. Each requiring destructive manual removal of soil samples while the water extraction and the isotope analysis are carried out in the laboratory. The most popular extraction methods are the cryogenic vacuum extraction (Orlowski et al., 2013), mechanical squeezing (Patterson et al., 1978), azeotropic distillation (Figueroa-Johnson et al., 2007), centrifugation (Kelln et al., 2001), microwave extraction (Munksgaard et al., 2014) and the direct vapor equilibration (DVE-LS) method (Hendry et al., 2015; Millar et al., 2018; Wassenaar et al., 2008a), showing valuable results.

However, these methods are labor intensive, expensive, susceptible to sample alteration through evaporation and disturb the soil system (Gaj et al., 2016).

On the other hand, different methods extract different water pools and even when using the same extraction methods. In case of the cryogenic water extraction, Orlowski et al., (2018) showed that results can even vary between laboratories.

This variety of extraction methods show the importance of a consistent and homogenized method for stable water isotopes analysis (Beyer & Dubbert, 2019).

1.3 Soil Water Retention

Plant water uptake is driven by the water potential gradient in the plant. Thereby, the accessibility of soil water to plants depends on the water binding tensions of the soil matrix, which differs due to the size of soil texture.

The water binding tension by the soil matrix is represented by the matric potential and describes the pressure magnitude in which water is retained in the soil matrix against the force of gravity (and is therefore indicated negatively). The matric potential is defined by the adsorption forces (adhesive and osmotic binding) of the soil texture (Amelung et al., 2018) which are much more present in structured soils with high surface area (clayish) than in coarse soils like sandy soils where capillarity dominates (Bengtsson et al., 1987).

The matric potential rises (gets less negative) with increasing soil water content and in contrast, decreases with decreasing water content. While sandy soils are characterized in percentage terms by a high proportion of coarse pores (>50 µm) resulting in matric potentials larger than -300 hPa, soils with high clay content are characterized by a high proportion of micropores (<0.2 µm) and matric potentials below -15000 hPa (Amelung et al., 2018).

Water retained in soils by matric potentials larger than -15000 hPa is considered as plant available. In contrast, water retained in soils with a matrix potential of less than -15000 hPa (hygroscopic water) is classified as unavailable to plants due to the limited capacity of plant water potential, although some desert plants (Halophytes) can still extract water from fine pores at matric potentials of -3×10^6 hPa (Amelung et al., 2018).

1.4 Water Infiltration and Distribution in the Vadose Zone

The water molecules are subject to multiple fractionation processes as they move through a forest ecosystem. As precipitation enters the soil- plant- continuum, the isotopic composition of water is altered by kinetic and equilibrium fractionation as it moves through the canopy of vegetation (Allen et al., 2015) during the phase change of evaporating water. The mixture of precipitation and altered throughfall water infiltrates the soil matrix and mixes partly with already existing water pools in the soil. Shallow soil water is affected by evaporation fractionation and thus enriched in heavy isotopes compared to deeper soil layers (Benettin et al., 2018; Sprenger, Leistert, et al., 2016).

Water movement described by the translatory flow (Hewlett, 1982; Horton & Hawkins, 1965) assumes that isotope signatures of mobile soil water follows the signal of local precipitation which displaces the resident soil water. In turn, it contributes to stream flow and groundwater recharge, presuming water to mix homogeneously throughout the soil profile.

However, the theory of translatory flow was challenged by (Brooks et al., 2010) when they found different isotope values in stream and xylem water. Their data implied a pool of tightly bound soil water (under relatively lower matric potentials) retained in the soil not participating in the translatory flow and thus not contributing to stream flow and groundwater recharge. The interpretation of their findings is that tightly bound soil water in small pores is only displaced by infiltrating precipitation after they were previously emptied by transpiration or after dry summers. They conclude that two separate water pools with different isotopic compositions exist, one of mobile soil water which contributes to groundwater recharge and stream flow, and one of bound soil water that plants preferably use for water uptake.

Differences in the isotopic composition of mobile and bound soil water isotopes were subsequently found by many other studies (Gierke et al., 2016; Goldsmith et al., 2012; Hervé-Fernández et al., 2016; Sprenger et al., 2018).
Sprenger et al., (2019) showed that even with rising groundwater tables, the saturation of the soil does not displace older, tightly bound waters and homogenize the isotopic composition of the soil water pools. By reviewing dozens of soil and plant water studies, Sprenger & Allen, (2020) conclude that a heterogenic water flow (e.g. preferential flow) into and through the unsaturated zone contributing to stream flow and groundwater recharge must be predominant. They assume that the observed isotopic differences of water pools are due to physical processes in heterogeneously structured soils (Sprenger & Allen, 2020).

The extent in which mobile and bound soil water pools mix based on their isotopic composition are still highly debated among ecohydrological studies (Berry et al., 2018; Beyer & Dubbert, 2019; Sprenger, Leistert, et al., 2016). Since several fractionation effects due to different physicochemical soil properties remain unclear, especially in natural ecosystems.

The ongoing debate on the interaction of mobile and bound soil water highlight the importance of choosing the right extraction method for the chosen research question and being cautious in interpreting the origin of the measured stable water isotopes, as well as the need for high-resolution spatiotemporal isotope measurements.

1.5 Impact of Plant Species on Soil Water Infiltration and Distribution

While isotope fractionation processes clearly take place within plants (Zhao et al., 2016), it is wildly assumed that there is no fractionation through root water uptake (RWU) although, some studies have shown isotopic fractionation by roots for some coastal woody plant species (Ellsworth & Williams, 2007; Lin & da SL Sternberg, 1993; Zhao et al., 2016).

Another important water flux to consider is the hydraulic redistribution of soil water, a process in which water passively moves from moist to dry regions in the soil via the plant root system and mycorrhizal networks (Hafner et al., 2017; Richards & Caldwell, 1987). Whether there is a fractionation process by RWU or not, plants take up water from different soil depths following their root distribution, nutrient availability and water binding forces (Dubbert & Werner, 2019) and create preferential flow paths through their rooting system. This subsequently, leads to uneven distributed infiltration and redistribution of soil water and thus can change the isotopic composition in different soil depths.

Bolte & Villanueva (2006) investigated the effects of interspecific competition of fine root structure and spatial fine root distribution of European beeches (Fagus Sylvatica) and Norway spruces (Picea Abies). They found a significant shift in the distribution of beech fine roots from upper to lower soil layers as well as a higher root length and specific surface area in mixed stands, compared to pure stands. Spruce, in contrast, did not show any significant changes in the rooting system in both, pure and mixed stands. This suggests a flexible adaption for water and nutrient uptake by beech trees in competition with other species. Schmid, (2002) showed that roots of beech trees were over- represented in the rooting zone of mixed stands, indicating even a competitive displacement of fine roots of spruce trees. In addition, their results show that spruce trees developed a more superficially distributed root system in a mixed stand compared to pure stands. Their results support the highly competitive ability of beech trees in the rooting zone and in contrast, the conservative competition behavior of spruce trees.

1.6 Progress in Isotope Measurements

Considering all the fractionation processes and redistribution factors affecting soil water, more research on water distribution and infiltration patterns is required to understand the impact of physiochemical soil properties and plant species on the spatial and temporal variability of soil isotopes in natural ecosystem.

Based on the DVE-LS method by Wassenaar et al., (2008), new non-destructive in situ methods have been established in the ecohydrological community over the past decade (Herbstritt et al., 2012; Rothfuss et al., 2013; Volkmann & Weiler, 2014), offering the opportunity of high temporal resolution measurements of soil (and plant) water isotopes. Both methods are based on the principle of equilibrium fractionation. As a function of time, an equilibrium of the ratio of isotopes in liquid water and saturated water vapor is established at constant temperature in a closed system. While field- deployable laser spectroscopy enables the measurement of stable water isotopes in the water vapor, the linear relationship between equilibrated liquid and vapor water enables the calculation of the (liquid) soil water isotopes.

With the development and improvement of non- destructive in situ measurement techniques, new possibilities arise as the resolution of water stable isotope measurements grow in space and time. They enable isotope measurements in plants and soils with a resolution of less than one second. This allows the smallest changes in water isotopes to be recorded directly, providing new insights into the processes within the SPAC.

In this study we use the in situ “Diffusion Dilution Sampling” (DDS) design developed and tested by (Herbstritt et al., 2012; Volkmann & Weiler, 2014). Semi-permeable (hydrophobic but vapor- permeable microporous) membranes installed into the soil provide a gas-vapor exchange between air in the soil pores and a connected cavity ring down spectrometer (CRDS).

Since the new in situ method offers promising opportunities, further research is required to test the performance of this method in large experimental set ups in natural ecosystems with different plant species and soil types. Since several isotope fractionation effects are still unclear, high resolution isotope measurements could contribute to a better understanding of the interaction of different water pools. Which would enhance the understanding of mechanisms that influence the soil water infiltration and distribution. This highlights the demand of more holistic and interdisciplinary research in ecohydrological studies involving hydrologists, soil scientist and plant physiologists for a better understanding of processes in the SPAC.

1.7 Goal of the Study

We investigated the distribution and infiltration patterns of stable water isotopes (^{2}H and ^{18}O) in soil pore water under natural conditions in a 0.75 ha forest study site in the Blackforest, Germany. Therefore, we analyzed the spatial and temporal variability of the isotopic composition of precipitation, throughfall and soil water in the unsaturated zone. Furthermore, we analyzed the physiochemical soil properties soil texture, cation exchange capacity (CEC), pH, carbon to nitrogen ratio (C/N) as well as the volumetric soil water content (VWC), matric potential (MP) and soil temperature to evaluate the influence of these properties on the soil water isotopes. Additionally, we investigated the influence of the two tree species European beech (Fagus Sylvatica) and Norway spruce (Picea Abies) on the soil water soil water infiltration and distribution using soil water isotopes.

Our hypotheses were:

1. Different physiochemical soil properties affect the stable water isotope composition. (Soil texture, pH, C/N ratio, CEC, soil temperature, VWC and MP)
2. Different forest stand compositions have an impact on the soil water infiltration and distribution patterns.
   (Impact of RWU, rooting depth and distribution on infiltration patterns)

2. Methods

In the following chapter, we describe our study area and experimental set up as well as the methods used to analyze the physicochemical soil properties and soil water isotopes in our study. At the end of this chapter, we present the statistical methods we used to answer our hypotheses from chapter 1.7 Goal of the Study.

2.1 Site Description

The study was carried out on a 0.75 ha site established in the Black Forest near Ettenheim, Germany (48°15'15.9"N 7°55'27.4"E; 530 m a.s.l).

The site is a southwest facing forested slope (16°) with a mean annual temperature of 10,48 °C (highest average in August with 23,8 °C and lowest in January with 1,7 °C) and an annual precipitation of 1000 mm (DWD, 2021). The area is used for forestry and dominated by European beech (Fagus Sylvatica) and Norway spruce (Picea Abies). The soil is classified as brown soil from loessy flowing soil over red sandstone flowing soil (90 – 100 cm soil depth). It has a characteristic increasing clay content in the subsoil as a result of decalcification and new clay mineral formation (illites, montmorillonites). Likewise characteristic is the brown color of the B horizon due to the iron oxide goethite, which coats the mineral grains like a fine skin (GeoLa, 2021).

For our study, we defined 9 plots with three trees each, more precisely three plots with pure beech, three with pure spruce and three plots with mixed stands. The trees were about 60 years old and 15 m high. An overview of the site description is depicted in *Figure 1*.

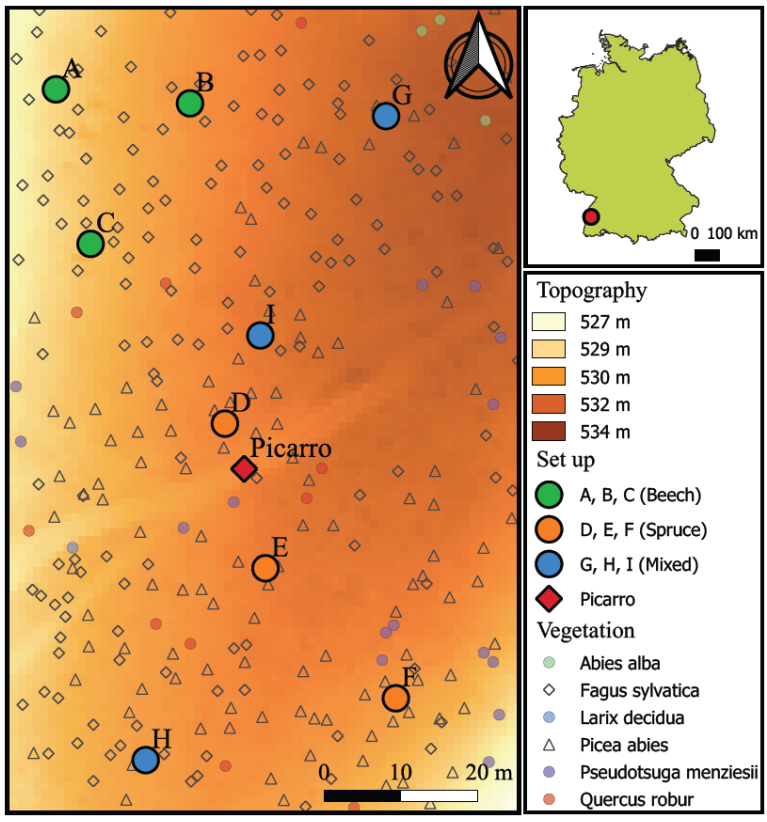

Figure 1: Overview of study site with location, set up, topography and vegetation types

2.2 Sampling

We installed a climate station at an exposed site 500 m northwest of the study site equipped with the following sensors in order to measure meteorological data:

Air temperature and relative humidity (CS215-L, Campbell Scientific Ltd., Bremen, Germany), precipitation amount (tipping bucket, 0,2 mm resolution Davis Instruments, Hayward, USA) photosynthetic active radiation (PAR) (LI-1500, LI- COR Biosciences GmbH, Bad Homburg, Germany) and windspeed (WindSonic, Gill Instruments Limited, Hampshire, United Kingdom). All data was obtained in 5-minute resolution.

At the study site, we installed several sensors in the soil and on the soil surface at each of our nine plots. A schematic overview of the set up for one representative plot is shown in *Figure 2.*

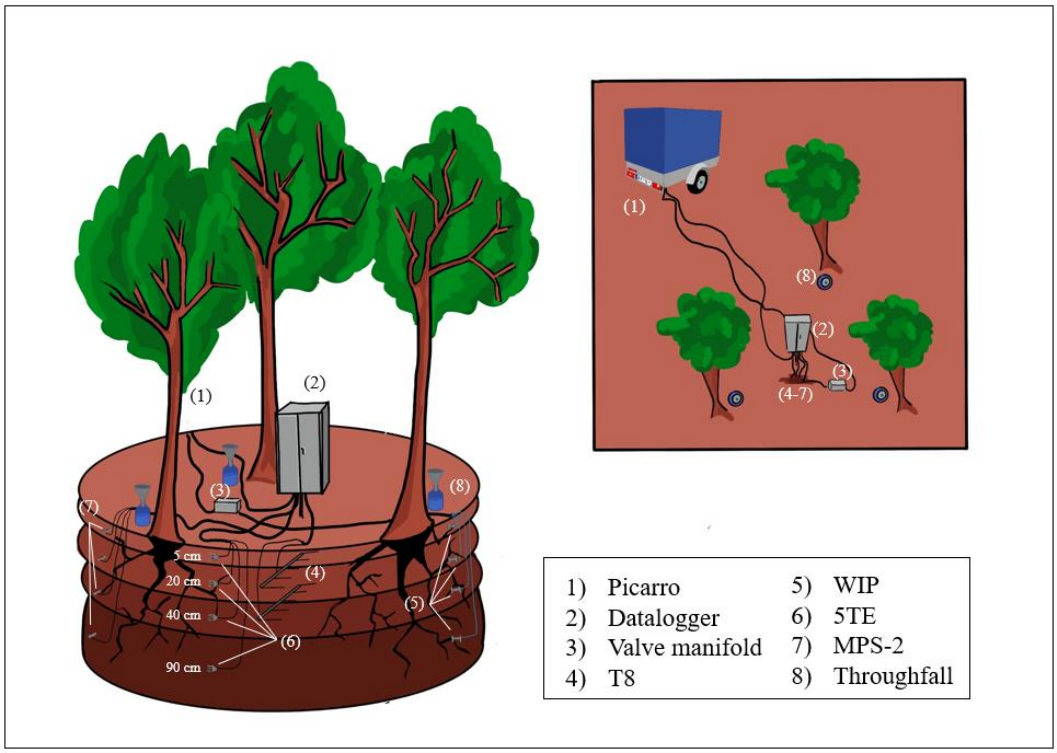

Figure 2: Schematic overview of sensor set up at an example plot

We installed three throughflow samplers (8) at each plot to measure the spatial variability of throughfall. We also installed a precipitation sampler next to the climate station to record the isotopic composition of precipitation. We collected the samples and measured the volume on a weekly basis in the field (or less frequently during dry periods) while we analyzed the isotopic composition in the laboratory by a CRDS (L2130-i, Picarro, Santa Clara, Inc., USA).

In addition, we measured volumetric water content (VWC), matrix potential (MP), and soil temperature (T soil) continuously at each plot in four soil depth profiles (5, 20, 40, and 90 cm soil depth). All sensor measurements were logged in 10 min intervals by a data logger (2) (CR100, Campell Scientific, Bremen, Germany). We installed a total of 36 VWC (5 TE, METER Group, Inc. USA) sensors (6) (range:1-80% , resolution: 0.08%, accuracy: ± 3%) (Decagon Devices, 2008) and 36 MP (MPS-2, METER Group, Inc. USA) sensors (7)

(range: -5000 to -50 hPa, resolution: 1 hPa, accuracy: ± 25%) (Decagon Devices Inc, 2011) to measure matric potential. Furthermore, we installed 12 T8 (Solutions, 2017) MP sensors (4) (range: -850 hPa to 0 hPa, accuracy: ± 5 hPa) at our plots (A,C,E,F,H,I) in 20 and 40 cm soil depth with the aim to compare the measured values of both matric potential sensors. The T8 sensors are significantly more sensitive than the MPS-2 sensors, while the MPS-2 devices are capable to measure much smaller water potentials than the T8 sensors. In addition to the VWC, the 5TE sensors also measure the soil temperature (range: -40 - 50 °C, resolution: 0.1 °C, accuracy: ± 1%).

Analogous to the VWC and MP sensors, we installed 36 in-situ water isotope probes (WIPs) (5) according to (Volkmann & Weiler, 2014) at each soil depth to extract soil pore water vapor. Through valve manifolds (3), we connected the probes to a CRDS locked in a trailer (1) at the study site, measuring the soil pore water isotope compositions at a high temporal resolution, varying on specific criteria (see chapter 2.4.2 In Situ Isotope Probes).

2.3 Soil Analysis

In addition to the continuous measurements, we analyzed soil samples to determine the cation exchange capacity (CEC), carbon to nitrogen ratio (C/N), pH and soil texture. We took soil samples from each plot and soil depths (5, 20, 40, 90 cm) during the installation of the sensors and WIPs in April 2021 and analyzed them at the laboratories of the University of Freiburg, while we determined the soil texture in the field by finger test.

2.3.1 CEC

We choose soil samples from three plots (C,F,I), each being representative of a pure or mixed stand and analyzed the CEC at the Chair of Soil Ecology. The applied method was based on (DIN 19684 Teil 8) but instead of $BaCl_2$ we used $SrCl_2$. Therefore, we oven dried the soil samples at 104°C for 24 h and added 5 g of each sample to a 100 ml volumetric flask with funnel and a pleated paper filter. Afterwards, we added $SrCl_2$-triethanolamine solution (26.66 g $SrCl_2$, 6 ml H_2O and 22,5 ml $C_6H_{15}NO_3$ at a pH of 8.2 to the sample until the volumetric flask was filled. During the reaction, the soil colloids became completely covered with the artificially added strontium cations (which are originally not present in the soil) while the cations which were previously bound to the colloids soil sample were released. Subsequently, we determined the exchanged cations by an atomic absorption spectrometer (AAS).

2.3.2 C/N

In order to determine the C/N ratio, we separated the soil samples from fine roots as shown in *Figure 3.* Afterwards, we filled the samples in 1.5 ml centrifuge reaction vessels and added an iron mumble. We treated the samples with a vibrating mill (MM400, Retsch GmbH, Haan, Germany) for fine grinding at a frequency of $30s^{-1}$ for 10 minutes. We subsequently burned them at 1020°C in a tungsten and copper filled tube (Oldenburg, 2008). In this process, the carbon compounds and CO_2 oxidized, and the nitrogen compounds were

reduced to N_2 via nitrogen oxides. In an integrated gas chromatograph, the gas mixture was separated and measured with the aid of a thermal conductivity detector. The analysis was performed at the Chair of Ecosystem Physiology.

Figure 3: C/N sample preparation: Removal of fine roots (left) reaction vessel with iron mumble (center) and vibrating mill (right)

2.3.3 pH

We determined the pH value of our soil samples in August 2021, at the laboratory of the Chair of Hydrology. We applied the method based on (DIN 19684 Teil 1, 1977) but used distilled water instead of $CaCl_2$ (same volume, same pH). In order to measure the pH of the solid soil samples, we first homogenized 10 g of each sample in a 50 ml vessel with 25 ml distilled water (EC= 0.05 µS/cm, pH= 6.0, Purelab flex) using a laboratory shaker (HS 250, JANKE & KUNKEL) with 100 motion/min for 24 h to separate solid matter from liquid, see *Figure 4.*

We then measured the pH value of the separated liquid. We previously calibrated the voltmeter (pH meter, WTW, SenTix) with standard buffer solutions of pH 4.0 and pH 7.0.

Figure 4: Soil sample preparation and measurement of pH values: Laboratory shaker for homogenization (left), liquid mixture separated from solid mixture (center) and pH meter (right)

2.3.4 Soil Texture

We estimated the soil texture by finger test. The criteria for the soil texture determination are plasticity, lubricity, roughness and rollability of a soil sample. We moistened the samples well without oversaturating them. Subsequently, we rolled the samples between the palms of the hands or triturated them between the fingertips. We estimated the soil texture by comparing the behavior of the soil sample with respect to the above criteria to the determination key see (Oldenburg, 2008).

2.3.5 Soil Water Retention Characteristics

The relation of volumetric water content and matric potential provide information on the water retention characteristics of the investigated soil. In order to illustrate the heterogenetic water retention characteristics of our studied soils, we applied the van Genuchten model (Van Genuchten, 1980) to fit soil water retention curves (SWRC's) to the measured volumetric water content and matric potential values. Due to the higher sensitivity of the T8 sensors compared to the MPS-2 sensors, we applied the model for the plots A,C,E,F,H and I (as they are the only ones with installed T8 sensors).
The SWRC after van Genuchten is an empirical model based on equation 1:

$$\theta = \theta_r + \frac{(\theta_s - \theta_r)}{[1 + (\alpha \times h)^n]^m} \quad (1)$$

where θ is the soil water content (Vol.%) , θ_s the saturated and θ_r the residual soil water content (Vol.%.). α is the air entry pressure (cm^{-1}) and h the matric potential or pressure head (hPa or cm (H_2O)). $m = 1\text{-}1n^{-1}$ with n as a measure of pore size distribution. M and n are both dimensionless parameters that are responsible for the shape of the curve. The parameters with the best fit were estimated using "SWRC Fit" (SWRC Ft, 2020) developed by (Seki, 2007). In addition, SWRC's of typical clay loam, silty loam, and sandy loam soils were added to the applied model with van Genuchten parameters derived from (Gootman et al., 2020; Nemes et al., 1999; Tomasella & Hodnett, 1996) to see if our model results show similar characteristics.

2.4 Stable Isotope Analysis

For the investigation of deuterium (^2H) and oxygen-18 (^{18}O) concentrations, we calculated the isotope ratio R_{sample} of the particle numbers of the heavy isotope (S_h) and the light isotope (S_l) of a sample S as their quotient:

$$R_{sample} = \frac{S_h}{S_l} \quad (2)$$

In order to eliminate small numerical values, as the heavy isotopes occur much less frequently under natural conditions than the light isotopes, we express the ^2H and ^{18}O concentrations in units of parts per thousand (‰) relative to a standard. For atmospheric applications, the delta (δ) notation is used for isotope quantification, with the ratio of the

measured heavy to the light isotope R_{sample} and for this study, the isotope ratio of the Vienna Standard Mean Ocean Water (VSMOW) $R_{Reference}$, which is published and updated regularly by the International Atomic Energy Agency (IAEA) in Vienna.

$$\delta = \left(\frac{R_{sample} - R_{Reference}}{R_{Reference}} \right) \times 1000 \text{ ‰} \quad (3)$$

To properly interpret water fluxes in soils under natural conditions, it is necessary to determine the isotopic composition of precipitation and throughflow, which along with groundwater and subsurface flow are the original sources of soil water. Throughfall and water in shallow soil layers are affected by kinetic fractionation through evaporation and thus become enriched in heavy isotopes compared to the initial source.

Evaporation is the transition of liquid soil or surface water to vapor phase. Kinetic fractionation is an isotope fractionation process that separates stable isotopes based on their different masses and thus the thermally induced atomic transport (diffusivity).

Oxygen has a higher atomic weight than hydrogen, thus the isotopologue $^{1}H_2{}^{18}O$ is less likely to change from the liquid phase to the vapor phase than the $^{1}H^{2}H^{16}O$ -isotopologue under nonequilibrium condition (as in our atmosphere)- (Craig, 1961; Horita et al., 2008). Therefore, the relation between $\delta^{2}H$ and $\delta^{18}O$ of water under the influence of kinetic fractionation due to evaporation deviates from the GMWL and LWML (Sprenger, Leistert, et al., 2016). This deviation of the ^{2}H and ^{18}O relation was defined by (Dansgaard, 1964) as the deuterium excess (d- excess):

$$\text{d-excess} = \delta^{2}H - 8 \times \delta^{18}O \quad (4)$$

The determination of the d-excess and thus the influence of evaporation on the isotopic composition of water in shallow soil layers is important to consider, when trying to estimate water fluxes in the soil in consideration of mixing processes.

2.4.1 Direct Water Vapor Equilibration

In addition to the in situ isotope measurements, we took three soil core samples (dates: 07.16.2021, 08.17.2021, and 10.05.2021) for destructive isotope analysis. Therefore, we used a geological drill (length: 1 m, diameter: 2.8 cm) to take soil samples at 5, 20 and 40 cm soil depth. Approaches of deeper sampling failed due to the high rock content with increasing soil depth. We filled the soil samples (each of about 30 - 40 g) into 500 ml aluminum- coated bags (WEBAbag CB400-420siZ, Weber packaging GmbH, Güglingen, Germany). In accordance with the equilibration bag method after (Wassenaar et al., 2008b), we filled the sample bags with dehumidified air in the laboratory at the Chair of Hydrology and permanently sealed them by heat using a sealing tong (Weber Packaging GmbH). In parallel, we filled three lab internal reference standard waters (see *Table 1*) into 1000 ml bags and treated them in the same way as the soil samples.

We stored all bags in the laboratory at constant 20 °C to equilibrate for 48 h. After the equilibrium of the soil pore water and the water vapor inside the bags, we punctured the

sample bags via a hollow needle connected to the inlet port of a CRDS (L2120-I, Picarro, Santa Clara, Inc., USA). The water vapor of the bags was directed into the CRDS via an integrated vacuum pump at a constant intake rate of 35ml min^{-1}. The CRDS then measured the moisture content and isotope composition of the water vapor. The measured moisture and isotope composition stabilized after 5-8 minutes. For each sample, we took the average moisture and isotope values within a 90 s interval (in compliance with the threshold values see *Table 2).*

In addition to the soil sample bags, we measured the bags with the reference standard waters three times each (at the start and at the end, as well as in the middle of the measurement process). The measurements of the standard waters were needed in order to correct the measured isotope values of the water vapor to liquid values. Our approach of the vapor- liquid correction is shown in (chapter 2.5.1 Vapor- liquid Correction). Since the soil samples and standard waters were measured at the same moisture content, we omitted the moisture correction for the equilibration bag method.

Table 1: Standard waters at the Chair of Hydrology, University of Freiburg

Reference standard water	**δ^2H (VSMOW‰)**	**$\delta^{18}O$ (VSMOW‰)**
NS	0.47	0.07
WEK	-65.99	-9.5
FSM	-125.84	-16.61

2.4.2 In Situ Isotope Probes

For in situ isotope measurements, we installed water vapor isotope probes (WIPs) following the design of "diffusion dilution sampling" (DDS) introduced by (Volkmann & Weiler, 2014). We built and tested all probes in the lab at the Chair of Hydrology.

A schematic structure of the probes is given in *Figure 5*. Key element of the probes was a semi-permeable (hydrophobic but vapor- permeable microporous) cylinder (membrane head) (C) made of PE with a pore size of 10 µm (Porex Technologies, Aachen, Germany). The membrane head had a length of 50 mm and an outer diameter of 10 mm. Water vapor in the soil air passed through the membrane while the hydrophobic material prevented liquid water to pass through (depending on the differential pressures).

Soil pore water vapor exchanged under equilibrium conditions with the air and vapor mixture inside the membrane head. The membrane head was connected to a mixing chamber (B) with three attached gas transport lines which were protected by an insertion shaft (A). The sampling line (D) was connected to a CRDS (L2130-i, Picarro, Santa Clara, Inc., USA) water vapor isotope analyzer with a regulated constant intake rate of 27 ml min^{-1} through an integrated vacuum pump.

A second line in the mixing chamber, the dilution line (E) delivered dry air to the mixing chamber in order to control dilution of the sampled air and vapor mixture, regulated by a mass flow controller (GFC17, 0-500ml min^{-1}, Analyt- MTC GmbH, Müllheim, Germany). The dilution line ensured that the air inside the membrane head and the water outside of the

membrane head can exchange under equilibrium conditions while flushing the sample line to remove pre-existing air from the system. If the dry air supply rate provided by the dilution line was smaller than the intake rate of the sampling line, soil pore water vapor advects through the membrane based on the applied pressure gradient and moves from the membrane head into the mixing chamber. By controlling the dilution rate, we regulated the vapor-mixing rate with the advantage of preventing condensation in the gas transport lines without providing a cost and energy intensive heating system.

The third transport line, the through-flow line (F) was implemented to supply dry air directly into the membrane head. The through-flow line was regulated by a second mass flow controller (GFC17, 0-500ml min^{-1}, Analyt- MTC GmbH, Müllheim, Germany) and compensated differences of intake and dilution rates to avoid pressure gradients at the membrane surface. All three transport lines were made of fluorinated ethylene propylene (FEP) with an outer diameter of 1.59 mm and an inner diameter of 0.75 mm (Techlab GmbH, Braunschweig, Germany).

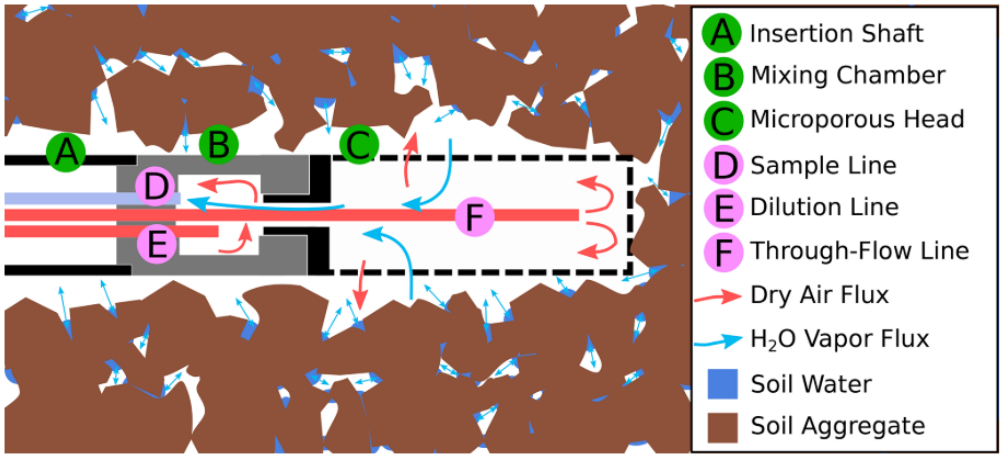

Figure 5: Schematic overview of the structure of a WIP taken from (Seeger & Weiler, 2021)

We connected the transport lines of each WIP to the mass controllers and the CRDS by valve manifolds (Horst Fischer GmbH, Gundelfingen, Germany). To enable the activation of a manifold, we augmented each manifold with two-way electric valves (EC-2M-12, Clippard, Cincinatti, USA). Transport lines and valve manifolds were connected by flangeless fittings (XP-220, IDEX, Lake Forest, USA) and the dry air supply (50 l compressed air bottle) with the mass controllers by stainless steel fittings (Swagelok, Solon, USA). In order to protect the CRDS and its peripherals, we installed the set up in a waterproof trailer (*Figure 6*) with power supply from a windmill at approximately 500 m distance.

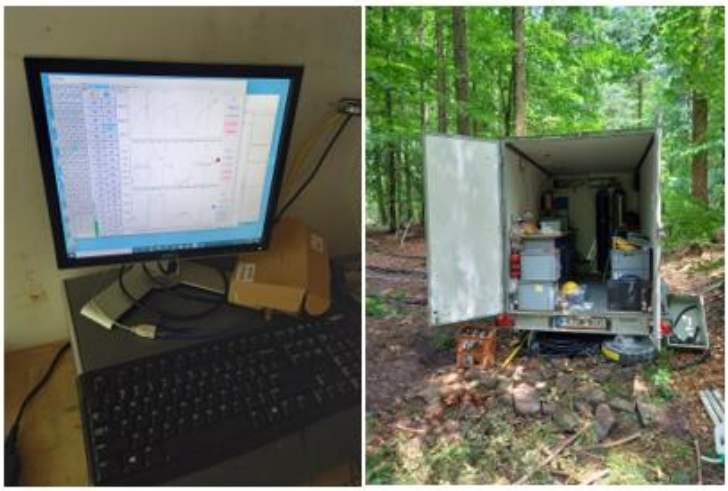

Figure 6: Picarro set up in waterproof trailer

We regulated the flow rate of the mass flow controllers by two independent analogue voltages, controlled by an Arduino custom built circuit board, capable of switching between the electric valves. In total, we built nine valve boxes (each containing an Arduino board and a valve manifold, fixated by a 3D printed bracket and silicone) as depicted in *Figure 7.*

Figure 7: Arduino board and valve manifold system

We connected all nine Arduino boards to the CRDS via LAN connection to ensure power and controlling. At each plot, we bundled the gas transport lines of each individual WIP via the valve manifolds which we in turn connected to the CRDS and mass flow controllers via three transport lines for each plot.

The control of the Arduino boards and the interpretation of the log files of the CRDS were run by a customized software GUI (Phyton), enabling a largely automated measurement process. A USB modem (E531, Huawei Technologies, Shenzhen, China) connected to the CRDS transmitted the measurement results to an FTP server. The automated system was developed in accordance to (Seeger & Weiler, 2021).

We controlled the measuring and flushing of the WIPs by activating the electric valves of each gas transport line of a probe. Starting with a flushing period where the input rate of the dilution lines equaled the intake rate of the sample line (in our case 27 ml min^{-1}), while we set the through-flow rate to zero ml min^{-1}. The duration of the flushing period depended on the overall tubing length (total length: 810 m for all gas transport lines, maximum flushing period: 60 min). The flushing period was followed by a measurement period by

reducing the dilution flow rate to 7 ml min^{-1} and increasing the throughflow rate to 20 ml min^{-1}, considering the total of both rates to equal the constant intake rate of the CRDS in order to avoid pressure gradients between the probes and the surrounding soil pores.

If the raw values measured by the CRDS approached a stable plateau (in which the threshold values for the standard deviations for δ^2H, $\delta^{18}O$ and moisture content were stable, see *Table 2*) the average values of the last two minutes were logged. We set the maximum duration of the measurement period to 45 minutes. After each WIP measurement, as well as after 45 min without a stable measurement, the system automatically started to flush and measure the next probe, following a specified order.

Table 2: Threshold values of valid isotope measurements

Parameter	Threshold values standard deviation
H_2O (ppmV)	150
δ^2H (‰)	0.9
$\delta^{18}O$ (‰)	0.3

2.5 Data Processing

We performed all statistical analyses using R (R Core Team, 2021) and RStudio (version 1.4.1717). For graphical visualizations, we used QGIS (QGIS Development Team, 2021; Version 3.14.16-Pi), ArcGIS Pro (CESRI, 2021; Version 2.9.0) and RStudio.

2.5.1 Vapor- liquid Correction

In order to correct the measured isotope values of the water vapor into soil water representative liquid values, we installed three reference standard waters at the sample site. We stored the three above mentioned lab reference standard waters (*Table 1*) in airtight containers of polyvinyl chloride (PVC-U) and embedded them in the soil to expose them to the same temperatures as the installed in situ probes. WIPs were installed in the air-filled headspace of the containers and connected to the valve box system to measure the water vapor of the standard waters regularly.

Instead of measuring the temperature at the place of equilibration (i.e. around the probe head), we relied on the assumption that the temperature is reflected by the water content of the measured vapor (Seeger & Weiler, 2021). We computed linear regressions between the measured vapor isotope values (δ_m) of the three standard waters (*Table 1*) and the vapor moisture contents (C_m). Thereupon, we derived slopes in order to correct the measured isotope values in the vapor to one reference moisture content value by equation 5 in accordance with Seeger & Weiler (2021):

$$\delta_v = \delta_m - \Delta_{C\delta} (C_r - C_m) \quad (5)$$

With δ_v being the corrected isotope value and $\Delta_{C\delta}$ the slope resulting from the linear regression between C_m and δ_m values of the three lab standards.

Since we knew the isotopic composition of our three lab standard waters in liquid phase, we were able to measure the relationship between liquid and vapor values after phase change. We used this relationship in order to correct the measured isotope vapor values to liquid values.

$$\delta_{l.x} = \frac{\delta_{v.x} - \delta_{v.L}}{\Delta_{LMH}} + \delta_{l.L} \quad (6)$$

with $\delta_{l.x}$ as the inferred liquid phase isotope value of a measurement x and $\delta_{v.x}$ as the moisture corrected vapor value of the measurement x, while $\delta_{v.L}$ is the moisture corrected vapor value of the light standard and $\delta_{l.L}$ the known liquid phase isotope value of the light standard. Δ_{LMH} is the derived slope between the liquid and vapor values of the standards and is obtained by equation 7:

$$\Delta_{LMH} = \frac{\delta_{v.L} - \delta_{v.M} - \delta_{v.H}}{\delta_{l.L} - \delta_{v.M} - \delta_{l.H}} \quad (7)$$

With $\delta_{v.M}$ being the moisture corrected vapor value of the medium standard and $\delta_{v.H}$ of the heavy standard. While $\delta_{l.L}$, $\delta_{l.M}$ and $\delta_{l.H}$ represent the known liquid water isotope values of each reference water standard (light, medium and heavy).

2.5.2 Meteorological Data Analysis

Based on the meteorological data that we measured at our climate station, we used the air temperature and relative humidity in order to calculate the vapor pressure deficit by equation 8:

$$\text{vpd} = 0.61078 \times \exp\left(\frac{-17.27\text{T}}{\text{T} + 265.5}\right) \times \frac{\text{RH}}{100} \quad (8)$$

Furthermore, we calculated the potential evaporation with the Penman- Monteith equation based on the daily averages of solar radiation, air temperature, relative humidity and wind speed, using the parameterization developed by the Food and Agricultural Organization (FAO) (R. G. Allen et al., 1994) by equation 9:

$$ET_0 = \frac{0.408\Delta(R_n - G) + \gamma \frac{900}{T+273} u_2 VPD}{\Delta + \gamma(1 + 0.34u_2)} \quad (9)$$

With ET_o as the reference potential evapotranspiration (mm day^{-1}), Rn being the net radiation at the climate station (MJ m^{-2} day^{-1}, in our case Rn = PAR/2.02, G the soil heat flux density (MJ m^{-2} day^{-1}),T the mean daily air temperature at 2 m height (°C), u_2 the wind speed at 2 m height (m s^{-1}), VPD the vapor pressure deficit (kPa), Δ the slope vapor pressure curve (kPa $°C^{-1}$) and γ the psychrometric constant (kPa $°C^{-1}$).

Based on the precipitation values we measured at the climate station, we determined wet and dry periods for our measurement campaign. We defined precipitation events by precipitation larger than 1 mm d^{-1} following the approach by (Demand et al., 2019).
Based on the defined precipitation events, we identified the weeks in which the most total precipitation accumulated in 7 consecutive days. We defined the last day of such a 7-day sequence as the wettest day of a wet period. In addition, we manually checked whether these days were associated with the observed matric potential values.

We performed the same approach for dry periods, with daily precipitation less than 1 mm d^{-1} and a time sequence of 14 days.

2.5.3 Variance Analysis

In order to investigate the impact of soil texture (contributing to Hypothesis 1) and different tree species (Hypothesis 2) on the isotopic composition of soil water, we defined two main groups and tested whether the isotope values within a group originated from the same population.

In the first main group ("Group by Soil"), we divided the plots into subgroups by predominant soil texture of all four soil depths (5, 20, 40 and 90 cm), resulting in two subgroups (see chapter 3.6 Variance Analysis).
In case of the second main group ("Group by Stand"), we formed three subgroups, one group for each pure stand (three beech and three spruce plots), and one representing the three plots with mixed stands.

Since main group 1 consists of two subgroups, we applied a two-sided t-test to check whether the isotope values of the two subgroups originate from the same population.

Main group 2 consists of three subgroups, therefore we performed a single factor variance analysis (ANOVA) in order to determine significant differences between the three populations.
We performed both tests for each soil depth (5, 20, 40 and 90 cm) separately.
To meet the criteria of the t- Test and ANOVA, we tested the isotope values of the plots within a subgroup for normal distribution by a visual check at the cumulative distribution function and in addition, by using the Anderson- Darling GoF- test with the R packages "MASS" (Venables & Ripley, 2002) and "ADGofTest" (Bellosta, 2011).
Subsequently, we tested the variance homogeneity by the Levene's- Test using the "psych and "car" packages in R (Revelle, 2021).

In the case of main Group 1 ("Group by Soil"): If one or more distributions within a subgroup were not normally distributed (and thus non-parametric), we applied the Mann-Whitney-U test instead of the t- test. If they were normally distributed, but the variances were heterogenic, we performed a Welch- test.

In the case of main Group 2 ("Group by Stand"): If the distribution within a subgroup proofed to be non-parametric or the variances were heterogenic, we applied the Kruskal-Wallis- test instead of the ANOVA. If the subgroups proofed to be significantly different ($p < 0.05$), we applied the Tukey HSD post-hoc test to determine which of the individual level comparisons were significantly different.

2.5.4 Regression Model

After conducting variance analyses, we investigated the reasons for potential differences in the isotopic composition of soil water among subgroups related to soil physicochemical properties. For this purpose, we applied a generalized linear model (GLM) for regression analysis to analyze patterns and magnitude of the effects of different physicochemical soil parameters (independent variables) on the soil water isotopes (dependent variables).

We aggregated the continuously measured values (with a 10-minute resolution) for volumetric water content, matric potential and soil temperature into daily medians to allow for comparison with the soil water isotope values that were available at a daily resolution. Since the WIPS were the most sensitive of the installed sensors and measured the least frequent, due to the threshold limits for valid values and the high number of probes connected to the CRDS, we had many data gaps due to sensor failure or invalid values. For this reason, it was first necessary to find days in which all the above-mentioned variables provided valid values.

The data were transformed by merging all daily medians of the continuously measured data with the available isotope values by matching dates. If a valid value was available for each variable on that day, the data series was marked. This was applied to plots C (beech), F (spruce), and I (mixed) throughout the entire measurement campaign. The GLM was reduced to these three plots because CEC data were only available for these three. The marked data series were supplemented with the associated constant pH, C/N, and CEC values, as we measured these only once, expecting no change in these values during the measurement campaign. In addition, we added the daily sum of precipitation to each data series.

All marked data series were stacked into a new data frame. Thus, a gap-free database was created for the GLM, in which the regression is calculated row by row only for the values of the variables measured on the same day.

3. Results

In the following chapter, we present our results of the analysis of soil physicochemical properties and soil water isotopes. First, we present the results of the soil properties and then those of the soil isotopes, starting with the equilibrium method followed by the in situ method. Then, the results of both methods are compared with each other and considered individually in more detail. In the last part, the results of the variance analysis and regression modeling are presented, which are discussed in the last chapter in order to answer our hypotheses.

3.1 Soil Analysis

The soil texture analysis by finger test revealed that the most soil horizons were in the range of a clay loam and silty loam texture, except for the Cv horizon of plot D, where we found a clay lens at 60 cm soil depth. The horizons showed a large variability between the different plots but also between the soil depth within each plot. No pattern in soil texture was apparent,

either by plot or by soil depth, indicating a high degree of heterogeneity of the studied soils. The results of the finger test are shown in the ternary diagram of the soil texture in *Figure 8.*

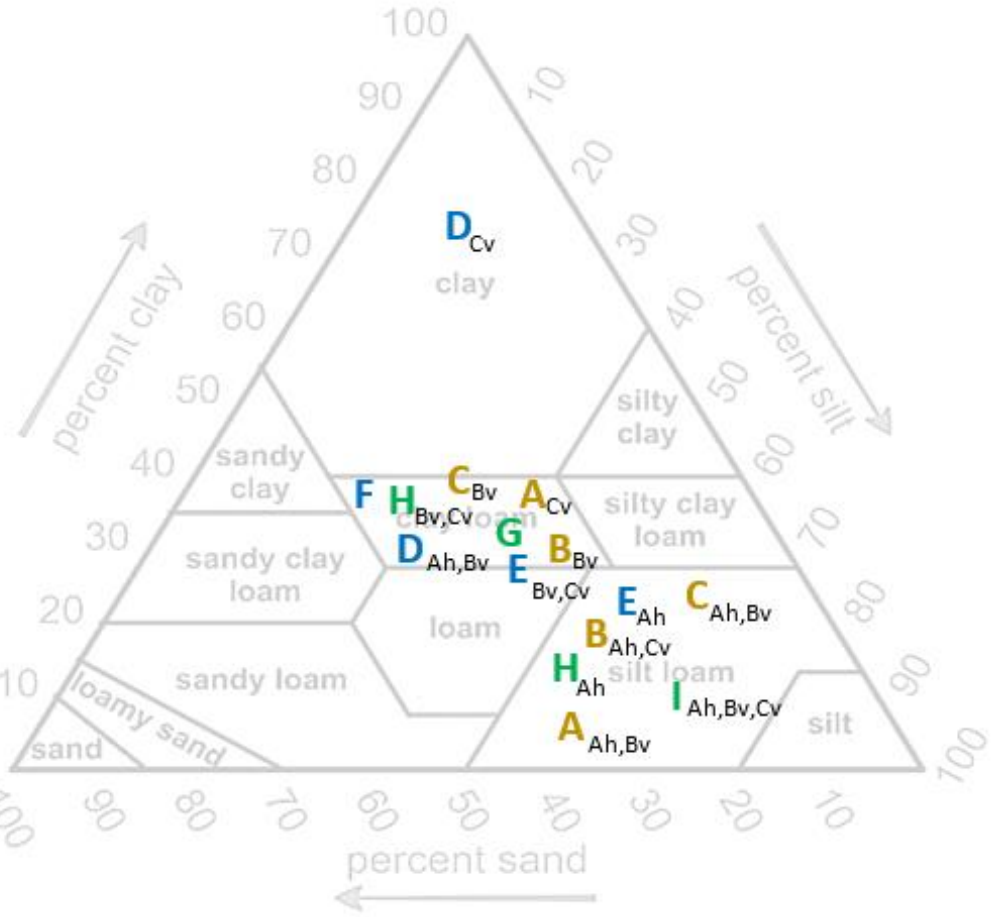

Figure 8: Ternary diagram of soil texture: Soil texture analysis of soil horizons (Ah,Bv,Cv) by finger test. Letters represent the different plots, colored by corresponding stand type (beeches in brown, spruces in blue & mixed in green). At Plot G & F: the texture at all three horizons are classified as clay loam

The measured pH values of all plots and soil depths are listed in *Table 3.* No values were avaible for Plot A and G at 90 cm soil depth. The results show that the soils under the spruce plots were the most acidic with an average pH of 4.65. The soils of the mixed plots had an average pH of 4.84 while the soils of the beech plots had an average pH value of 4.88.

Table 3: pH values of each plot and soil depth

Plot	pH at 5 [cm]	20 [cm]	40 [cm]	90 [cm]
A	4.61	4.77	4.72	
B	5.31	4.94	4.91	4.56
C	4.88	5.08	4.96	4.96
D	4.86	4.70	4.62	4.56
E	4.47	4.33	4.66	4.52
F	4.67	4.92	4.72	4.74
G	5.16	5.12	5.26	
H	4.48	5.01	4.83	4.70
I	4.52	4.86	4.66	4.61

The results of the CEC are shown in *Table 4.* Note that no H^+ values are available for Plot C and F at 5 cm soil depth. Most cation concentrations decrease by increasing depth, however Al^+ and H^+ increased with depth at Plot C and I.

Table 4: CEC values, sorted by plot and soil depth.

Plot	Soil depth [cm]	H^+ [molc/kg]	Al^{3+}	Ca^{2+}	Fe^{3+}	K^+	Mg^{2+}	Mn^{2+}	Na^+
C	5	20.80	9.000	30.99	0.060	2.447	17.64	6.488	0.390
	20	3.590	26.16	0.909	0.004	0.704	1.319	2.203	0.307
	40	34.95	24.02	2.877	-0.036	1.345	1.757	4.514	0.339
	90		33.58	2.700	-0.031	1.151	1.303	6.427	0.208
F	5	4.591	18.95	22.71	0.147	1.813	15.85	9.508	0.317
	20	3.893	32.25	2.323	0.068	0.947	2.271	2.203	0.242
	40	4.446	27.35	0.950	-0.002	0.948	0.950	1.479	0.224
	90	5.215	27.21	0.891	-0.036	0.887	0.584	0.844	0.227
	5	5.670	29.27	15.50	0.248	1.425	11.27	6.923	0.395
I	20	6.438	29.64	4.481	-0.001	1.105	2.507	5.410	0.283
	40	5.995	30.92	0.377	-0.025	0.069	0.513	1.138	0.194
	90		42.49	2.653	0.004	1.265	1.139	8.329	0.563

The results of the C/N ratio analysis are shown in *Table 4.* Note that no C/N values were available for Plot A and G at 90 cm and for H at 40 cm soil depth. For the most plots the C/N ratios decreased by increasing soil depth. The highest C/N ratios were found in the soils of the spruce stands and the lowest in the beech stands.

Table 5: C/N values, sorted by plot and soil depth

Plot	C/N at 5 [cm]	20 [cm]	40 [cm]	90 [cm]
A	18.16	14.21	8.95	
B	15.12	13.97	12.28	6.69
C	18.45	16.90	11.96	6.45
D	20.9	15.05	4.67	7.47
E	24.71	18.17	14.28	7.86
F	19.19	21.52	16.24	17.92
G	17.34	18.31	14.25	
H	16.93	19.8		3.25
I	21.74	17.26	12.41	5.38

3.2 Meteorological Data

The temporal dynamics of the daily precipitation, air temperature, photosynthetic radiation and vapor pressure deficit are depicted in *Figure 9*. The measuring campaign started on the 07.04.2021 and ended on 10.30.2021. The highest recorded air temperature was 32.88 °C on August 13th (2:45 PM) and the lowest at 1.075 °C on October 24th (06:45 am). The highest recorded daily precipitation was on July 13th with 39.6 mm. The PAR followed the trend of the air temperaure, declining from mid August till the end of October, with a maximum value of 216.3 mol $m^{-2}s^{-1}$ on July 09th (1:25 PM). The lowest measured VPD value was 0.54 kPa on August 13th (13:55 PM) and consequently increased with decreasing temperatures until the end of October with the highest value of 4.97 kPa on the 22nd of October (7:15 AM).

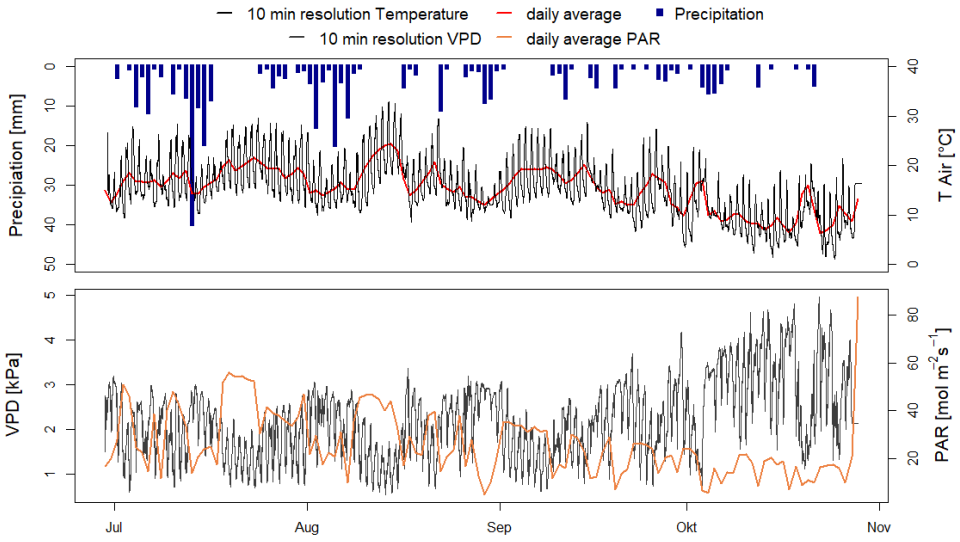

Figure 9: Meteorological data of the entire measuring campaign (07.04-30.10.2021). All data originates from the climate station, approximately500 m north west of the study site. Precipitation is shown in daily resolution, air temperature as daily averages (red line) and in 10 minute resolution (black line). PAR (orange line) is shown as daily averages and VPD (grey line) in 10 min resolution.

Following the approach described in chapter 2.5.2 Meteorological Data Analysis, we observed 43 days with precipitation events over the entire measurement campaign. The magnitude and distribution of these events were the basis on which we defined wet and dry weeks. In addition to weekly precipitation, the daily average matric potential of plot C at 40 cm soil depth on the last day of a given period (wet or dry) is given as a reference.

The wettest week was from 07.10.2021 till 07.16.2021 with a total of precipitation amount of 91.2 mm and a matric potential of -19 hPa. The second wettest week was from 08.01.2021 till 08.07.2021 with a total precipitation amount of 58.8 mm and a matric potential of -26 hPa.

The driest recorded week was from 09.23 - 09.30.2021 with a total precipitation amount of 7.8 mm and a matric potential of -809 hPa. The previous week had a total precipitation amount of 10.2 mm and a matric potential of -726 hPa. The second driest week was from 08.21-08.28.2021 with a total precipitation amount of 13 mm and a matric potential of -761 hPa at the last day of the dry period. The precipitation amount of the previous week was 6.8 mm with a matric potential of -536 hPa. The matric potentials of all plots were the lowest at the last day of the by rainfall events defined period.

3.3 Volumetric Water Content and Matric Potential

The spatiotemporal dynamics of the volumetric water contents of all nine plots are depicted in *Figure 10*, for the respective soil depth. The results are presented as daily averages and are grouped by stand type. The values show a negative trend from mid-August untill the end of the measurement campaign.

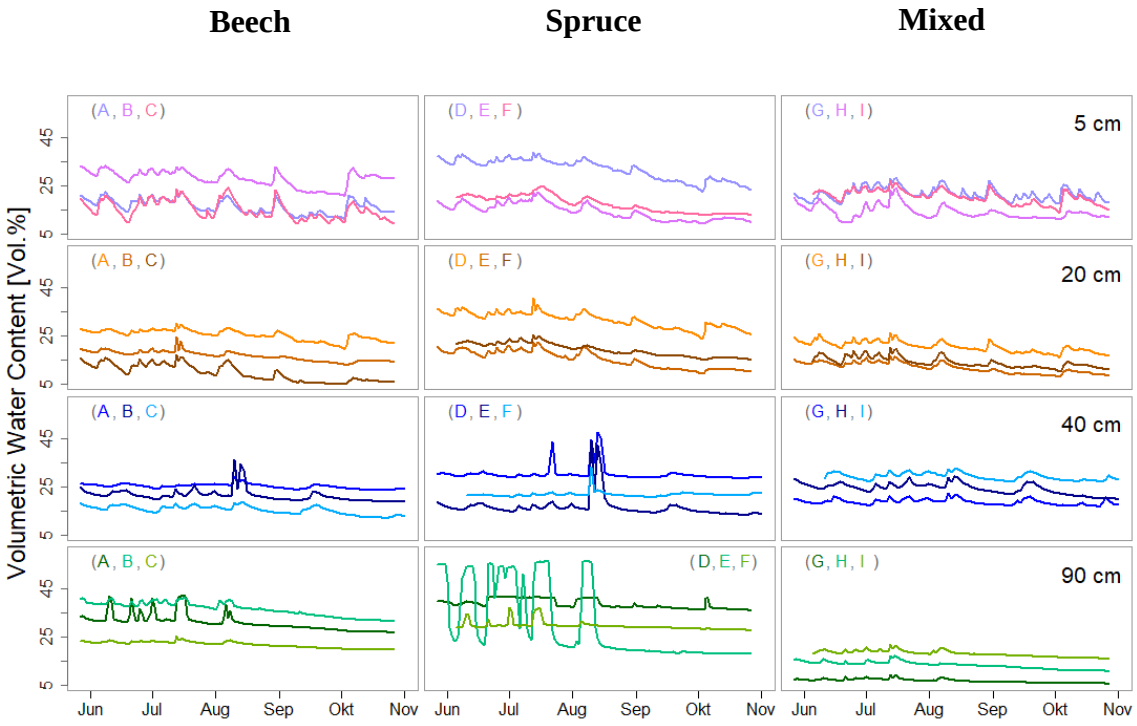

Figure 10: Temporal dynamics of volumetric water content of each plot and soil depth. Values are depicted as daily averages, color and letters represent plots and soil depths respectively

The average volumetric water contents of all nine plots increased with increasing soil depth, exept for the 20 cm layer with a slightly lower average value (19.18 Vol.%) than the 5 cm layer (20.61 Vol.%). In the 5 cm layer the values varied from 13.98 to 27.23 Vol.% and in 20 cm soil depth from 13.44 to 24.92 Vol.%.

While the highest daily fluctuations were observed in the upper soil layer (5cm), we measured the highest variability in 40 cm soil depth (from 17.59 to 32.48 Vol.%). This value was particularly influenced by the spruce plots (from 18.93 to 41.51 Vol.%), where plot E showed the highest variability (10.72 to 43.87 Vol.%). The same was true for 90 cm soil depth, with plot E standing out (18.03 to 56.23 Vol.%). The lowest observed variability was between the mixed stands in 90 cm, with values from 10.95 to 16.31 Vol.% and an average VWC of 13.63 Vol.%. On average, the mean variability in 90 cm soil depth ranged from 24.46 to 32.54 Vol.%, showing the lowest variability of all layers but at the same time the highest mean volumetric water content with 27 Vol.%. In the comparison between the different stands, the mixed stands showed the lowest variability and at the same time the lowest water content at most soil depths. A detailed overview of the VWC data is given in the Appendix, *Table A. 1.*

The different perfomances of the two matric potential sensor types are illustrated in *Figure 11*, separated by stand type. The MPS-2 sensors measured the lowest matric potentials up to -2700 hPa in 20 cm soil depth. Comparing the quantiles, the matric potentials measured by the T8 sensors showed a higher variability than the values measured by the MPS-2 sensors. The same performance behavior can be seen at 40 cm soil depth, see *Figure A. 1* in the Appendix. The medians of the measured values are close together, as demonstrated by the different boxplots. The highest values measured by the MPS-2 sensors are below -50 hPa and the lowest values measured by the T8 sensors are larger than -850 hPa, thus the values are within the measuring range of the individual sensor type.

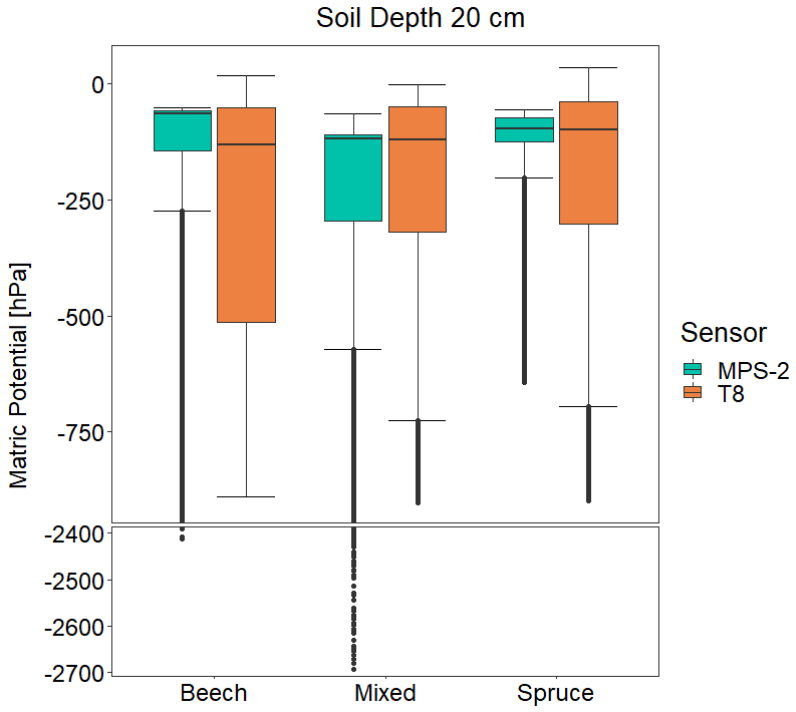

Figure 11: Performance comparison of MPS-2 and T8 Sensors (at 20 cm soil depth)

The spatiotemporal dynamics of matric potentials measured by the T8 sensors over the entire measurement campaign are shown in *Figure 12*. The depicted values are daily averages. All sensors showed a similar behavior, following the trend of the measured volumetric water contents (see *Figure 10)*. We measured relative constant values from June till mid-August, followed by a large decrease to lower matric potentials up to -850 hPa on Septmeber 10th (plot H) in 20 cm soil depth and -850 hPa on Septmeber 30th again, in 20 cm soil depth (plot H). All values of the six plots followed a similar trend both in the course and magnitude at 20 and 40 cm soil depths, except for plot E, F and I at 40 cm soil depth, with the same course, but a significantly lower magnitude. Between September and October, we measured larger matric potentials at plot E and F in 40 cm soil depth than in the upper 20 cm layer. We observed the largest difference between soil depths at plot F on October 03rd, with -850 hPa in 20 cm and -148 hPa in 40 cm soil depth.

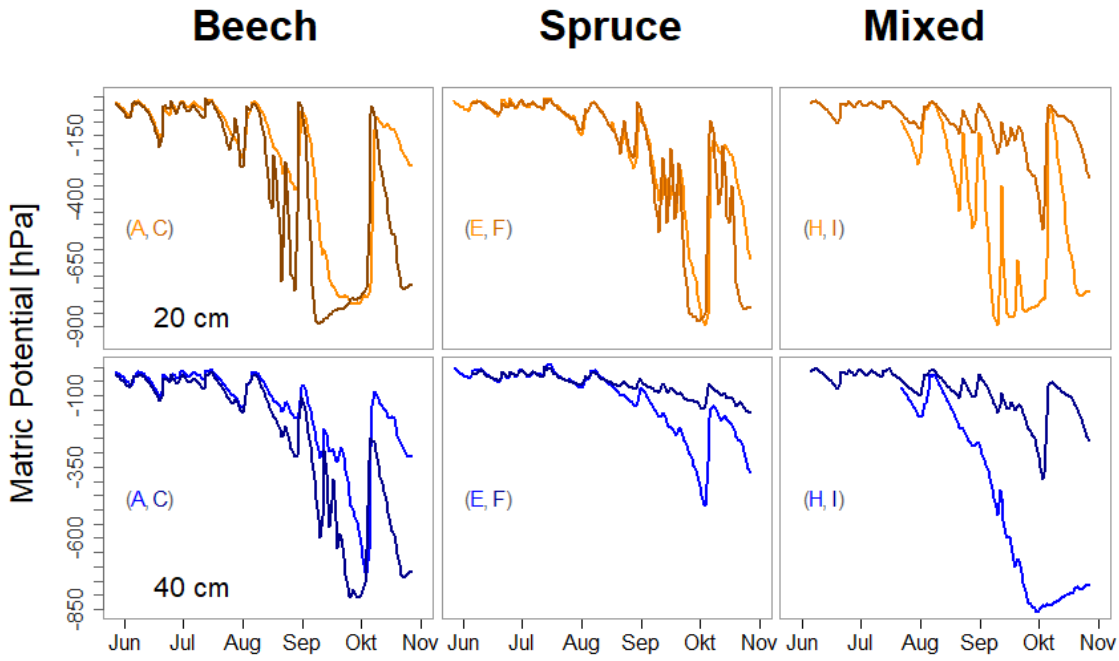

Figure 12: Spatiotemporal dynamics of matric potential measured with T8 sensors

3.4 Soil Water Retention Characteristics

Since the T8 sensors have a higher sensitivity compared to the MPS-2 sensors, the values of the T8 sensors were used in order to illustrate the relation of the observed volumetric water contents and matric potentials by modelling the soil water retention curves of our investigated soils. The results are depicted in *Figure 13*, showing the measured water content and matric potential values as well as the modelled soil water retention curves in 20 cm soil depth after van Genuchten. In addition, the SWRC's (also van Genuchten) of empirically determined silty loam, clay loam and sandy loam textures are shown, with derived parameters from literature (see chapter 2.3.5 Soil Water Retention Characteristics).

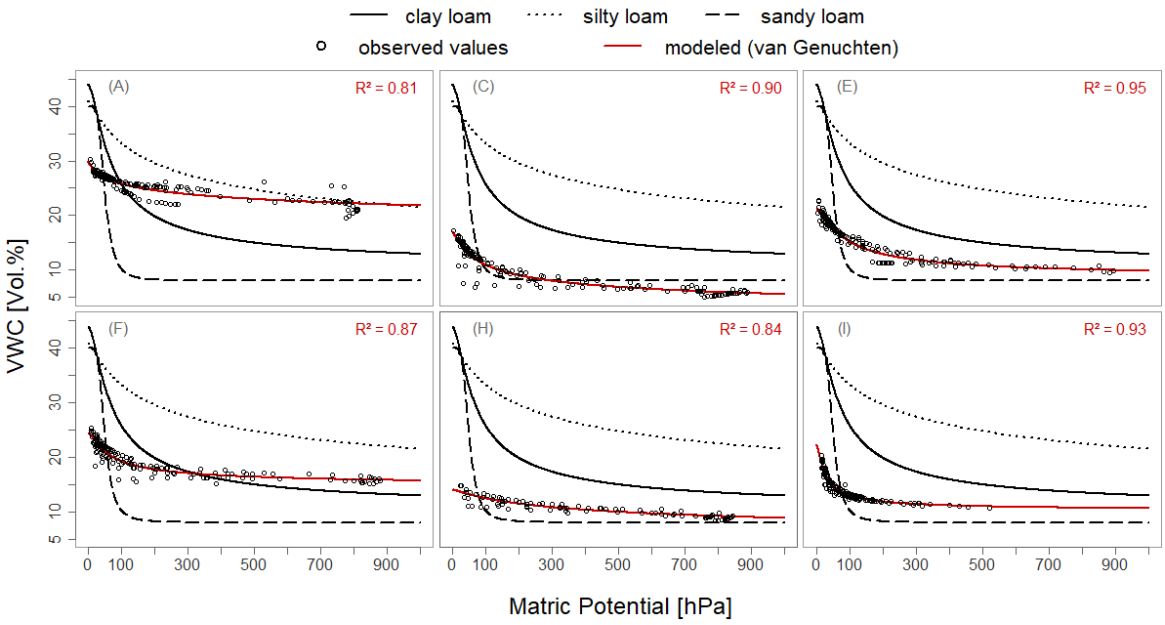

Figure 13: Soil water retention curves (red curves) of plot (A,C,E,F,H and I) at 20 cm soil depth, modelled with van Genuchten parameters. In addition, SWRC's with parameters derived from (Gootman et al., 2020; Nemes et al., 1999; Tomasella & Hodnett, 1996) for comparison.

A detailed overview of the derived and calculated parameters is shown in the Appendix in *Table A. 2*.

The modeled SRWC´s are within the range of the results from the reference literature. The curves of plot E, H and I lie between clay loam and sandy loam while the curves of plot A and F intersect the clay loam curve and fit between the clay loam and silty loam curves. Plot C shows the lowest water retention characteristics, even lower than sandy loam at volumetric water contents lower than 10 Vol.% and matric potentials smaller than – 300 hPa respectively. The best model fit was achieved at plot E with an R^2 of 0.95 and the poorest fit at plot A with an R^2 of 0.81.

3.5 Isotope Measurements

In order to answer our hypotheses, we investigated the behavior of the soil pore water isotopes under different tree stands and soil properties. Therefore, the analysis of the observed isotope values are key to this study and are given special weight later in the evaluation. For soil water isotope analysis, we applied two measuring methods (in situ and equilibration bag) that are subject to the same principle (direct vapor equilibration and laser spectroscopy).

In the following chapter, the results of all isotope measurements from both methods are presented to provide an overview of the spatiotemporal dynamics of the observed soil water isotopes values.

3.5.1 Equilibration Bag Method

The results of the liquid corrected isotope values measured with the equilibration bag method are presented in *Figure 14*, showing the depth profiles of δ^2H values taken on the three different dates.

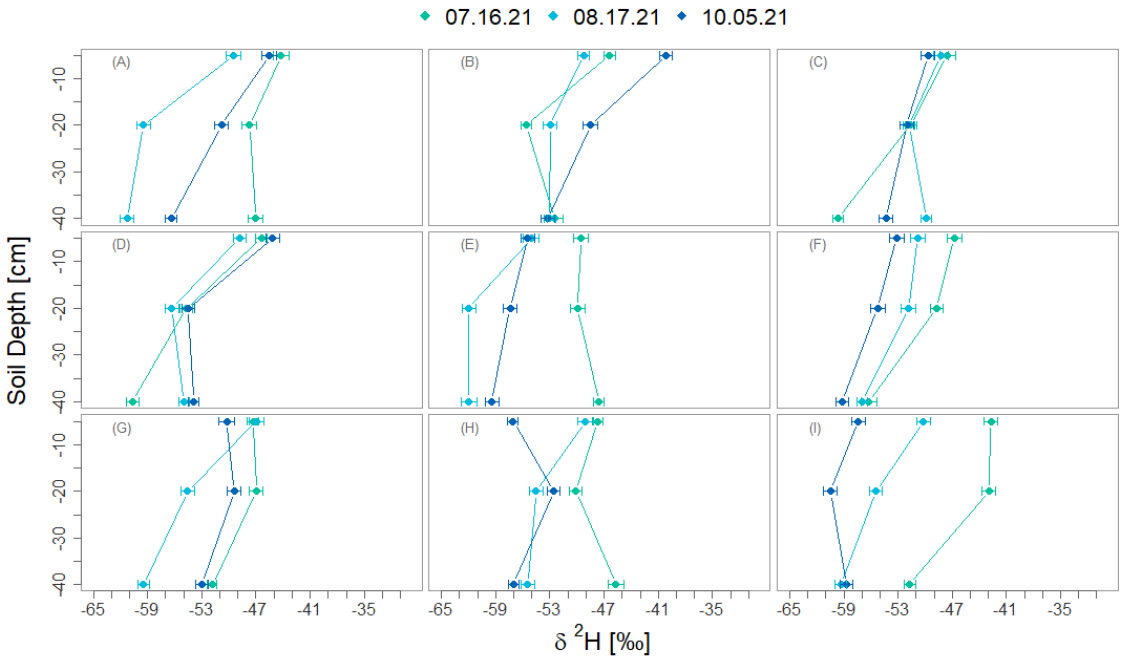

Figure 14: Depth profiles of δ^2H values with corresponding standard deviation (error bars). Values were measured with the equilibration bag method. Color marks the sample dates of each value. Letters stand for the respective plot. Connecting lines between the values of the three soil depths (5, 20, 40 cm) are interpolated

For most cases, the δ^2H values of the soil pore water decreased with increasing soil depth, showing a depletion of ^2H in deeper soil layers compared to the observed values near the soil surface.

Furthermore, the values varied strongly between the different plots but also within each plot and different sampling dates. Except for plot C at 20 cm soil depth with all three measured values being close to each other (-51.58, -51.80 and -52.02‰). The measurement on 07.16.2021 showed average δ^2H values of -50.24 ± 0.74‰ for the beech plots (A,B,C), -51.17 ± 0.74‰ for the spruce plots (D,E,F) and an average value of -47.36 ± 0.68‰ for the mixed plots (G,H,I). The measurement on 08.17.2021 received average δ^2H values of -52.83 ± 0.72‰ (beech plots), -55.41 ± 0.75‰ (spruce plots) and -53.50 ± 0.74‰ at the mixed plots. On the 10.05.2021, we measured δ^2H values of -50.07 ± 0.75‰ (beech plots), -54.83 ± 0.72‰ (spruce plots) and -55.10 ± 0.71‰ at the mixed plots. A detailed overview of the results is shown in the Appendix in *Table A. 3*, *Table A. 4* and *Table A. 5*. While there were no significant differences in standard deviation between stand types, the average δ^2H values in the soil water under the spruce plots were most negative at all three sampling dates, while the δ^2H values were most positive at the beech plots, however, this was not true for the $\delta^{18}O$ values.

In order to illustrate the spatial variability of the measured δ^2H values between the plots and soil depths, the results from the 08.17.2021 sampling are shown in detail in *Figure 15*.

The highest variability was observed between the spruce plots (-54.93 to -48.83‰ at 5 cm, -61.9 to -55.05‰ at 20 cm and -56.96 to -50.80‰ at 40 cm) and the lowest between the mixed plots (-50.18 to -46.96‰ at 5 cm, -55.43 to -54.53‰ at 20 cm and -59.47 to -55.46‰ at 40 cm). The beech plots showed a low variability in the 5 cm layer but a higher variability in the deeper layers. In general, the variability is the lowest at 5 cm soil depth increasing with soil depth.

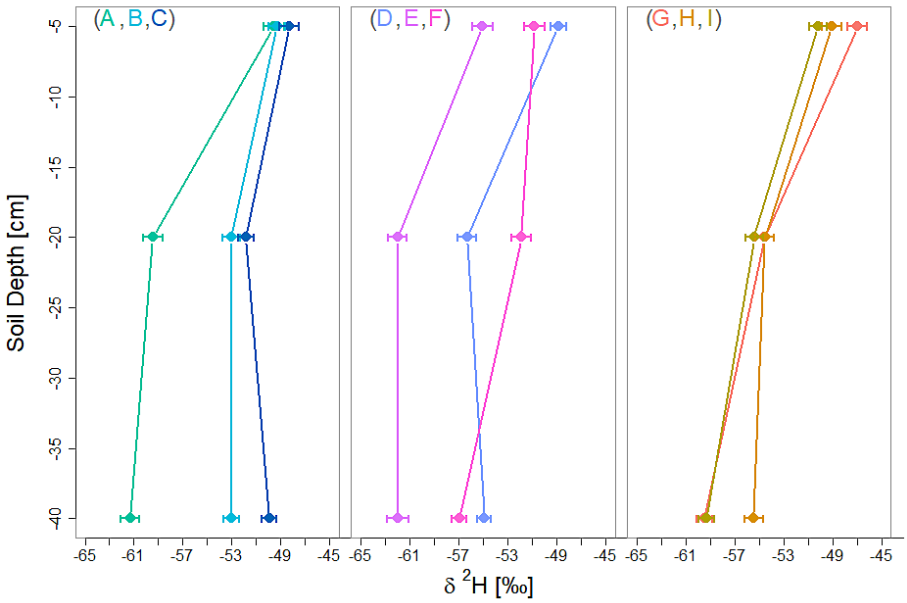

Figure 15: Depth profiles of spatial variability of δ^2H values measured with the equilibration bag method from 08.17.2021, letters and colors stand for the respective plot which are grouped by stand

3.5.2 In Situ Isotope Measurements

During the liquid vapor correction, we noticed that the measured $\delta^{18}O$ values in the vapor of the standard water NS and WEK were too close to each other and often even overlapped (see *Figure A. 2* in the Appenidx). Based on the clear difference in the liquid signatures, this should not be the case. The values should be differentiable even without correction as in the case of the δ^2H values see *Figure A. 3*. This unexpected behavior of the measured $\delta^{18}O$ values result in a poor model fit of a linear regression of the liquid and vapor values (R^2 = 0.64) see *Figure A. 4*. The linear regression of the δ^2H values however resulted in a good model fit (R^2=0.99) *Figure A. 5*. For this reason, we applied the liquid vapor correction only to ^2H and excluded ^{18}O from the evaluation.

The spatiotemporal course of all corrected (liquid correction and outlier removal) in situ δ^2H values for the entire measurement campaign is given in *Figure 16*. The measured values varied strongly both spatially and temporally. There were no values availabe for the spruce plots (D,E,F) between August and September due to sensor installation failures. In addition, some probes (G and H) failed frequently due to liquid water that penetrated the membrane head. Due to the clay lens, it was not possible for us to install a probe at plot D in 90 cm soil depth. Because to the large number of installed probes and the measurement criteria for valid values, the temporal resolution of each probe was limited to ± 1 day.

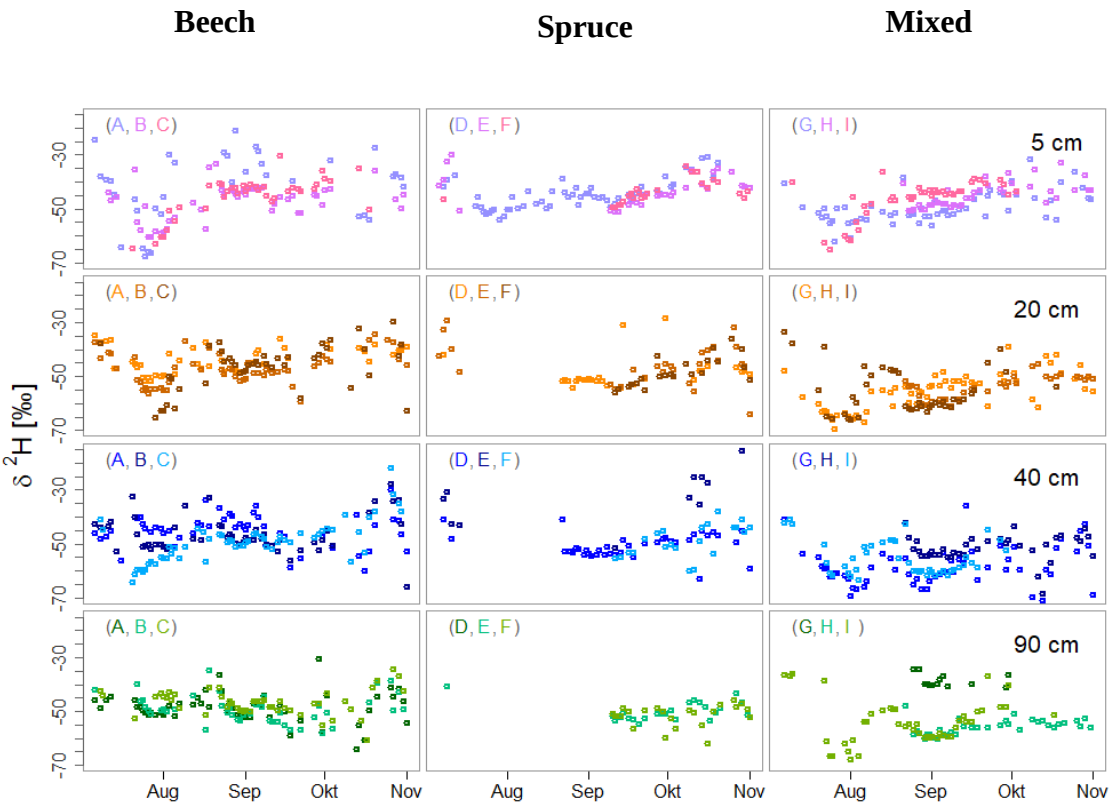

Figure 16: Spatiotemporal overview of all in situ δ^2H measurements. All plots of each stand are depicted in one graph, the plot values are differentiable by letter and color

The depth profiles of the δ^2H values measured by both methods (in situ and destructive) are depicted in *Figure 17* for the sampling date on 08.17.2021. Note that the destructive sampling was only carried out to a soil depth of 40 cm, while in situ probes were also installed in 90 cm soil depth. The results show that except for Plot A, the values measured by the two methods are close together and followed the same trend, getting lighter with increasing soil depth. Since not all in situ probes were measured on this day, some of the δ^2H values shown were measured on 08.16.2021 or 08.18.2021, but not further to account for temporal dynamics. Nevertheless, not all plots can be mapped, because in situ data was not available.

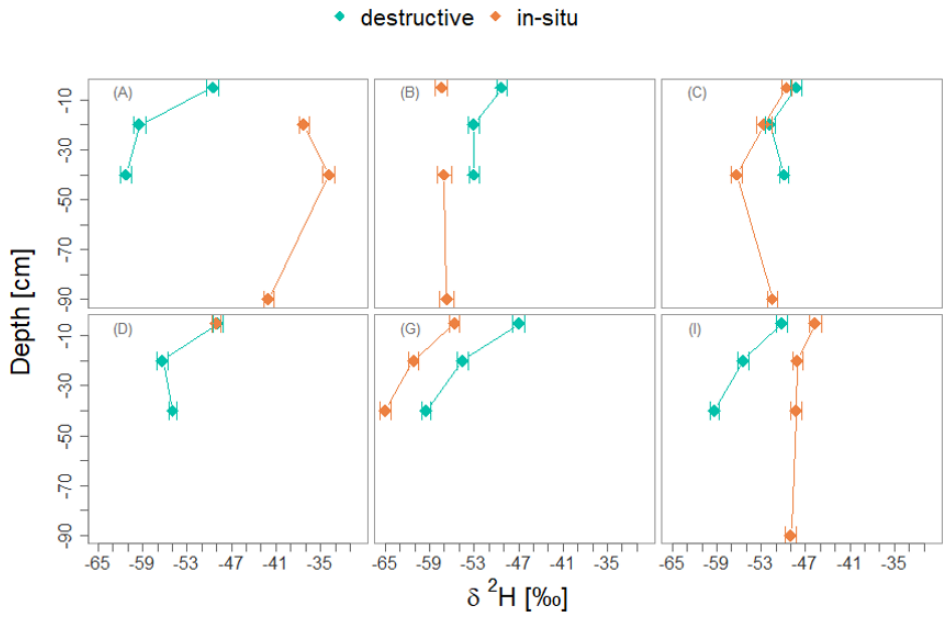

Figure 17: Comparison of destructive (turquoise) and in situ (orange) δ^2H values on 08.17.2021. Each plot is differentiable by letter.

The largest deviaton of measured values of both methods were at plot A in 40 cm soil depth with δ^2H values of -61.29 ± 0.77‰ for the destructive and -33.62 ± 0.84‰ for the in situ method. The smallest deviation was at plot D in 5 cm soil depth with values of -48.83‰ ± 0.67 for the destructive and ± -49.01 0.71‰ for the in situ method. The measurements and standard deviations of the two groups were not significantly different this day, with a two sided t-test result of (p> 0.05), thus accepting the null hypothesis that the values of both methods originate from the same population.

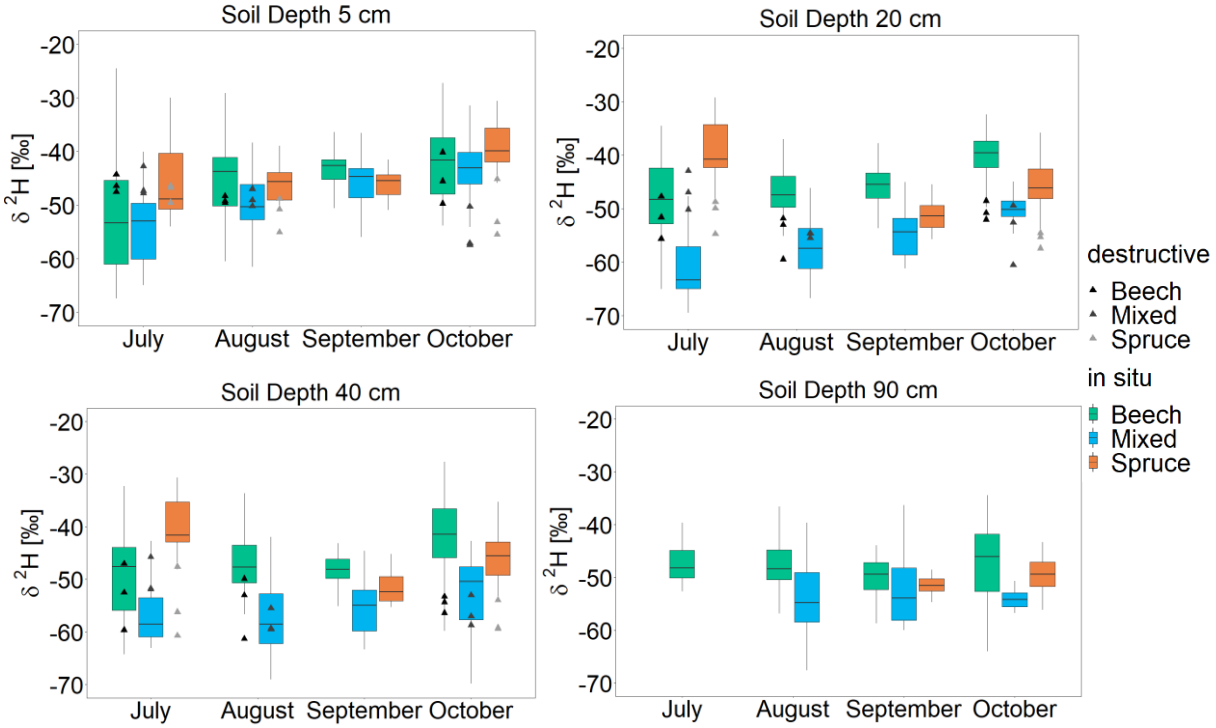

Figure 18: Boxplots of spatiotemporal soil water δ^2H values from in situ measurements and from the three destructive samplings (triangles) separated by stand type and differentiable by color

A comparison of all in insitu and destructive measured δ^2H values is shown in *Figure 18*. Boxplots are missing, where no or less than 15 in situ measurements were available.

The figure demonstrates that all values fluctuated over all months and soil depths. Further, the in situ measured δ^2H values in 5 and 20 cm soil depth became more positive over the time, while the values in 40 and 90 cm were more stable. The lowest observed variability was in September which was the driest month of the measurement campaign. The soil water of the mixed plots was isotopically most depleted whereas the soil water under the beech plots were most enriched except for July where we measured the most positive values under the spruce plots. Most of the destructive measured δ^2H values were within the quantile range of the in situ values but did not always overlap temporally.

3.5.3 Temporal Variability of Throughfall and Precipitation Isotopes

The evaluation of the measured δ^2H values of precipitation and throughfall showed a high temporal variability, but no significant trend ($p > 0.05$) over the measurement campaign. *Figure 19* shows the temporal course of the measured precipitation and throughfall δ^2H values, as well as the corresponding d-excess values. The throughfall δ^2H values were more positive with an average δ^2H value of -49.75 ‰ than the precipitation δ^2H values with an average of -56.75 ‰. This is also reflected in higher d-excess values with 10.57 for the throughfall samples and 9.88 for the precipitation samples. However, in some cases the δ^2H values in the precipitation samples were more positive and showed higher d-excess values compared to the values in the throughfall samples. The largest deviation of d-excess was on August 4th with a value of 8.44 for the precipitation and 11.11 for the throughfall sample.

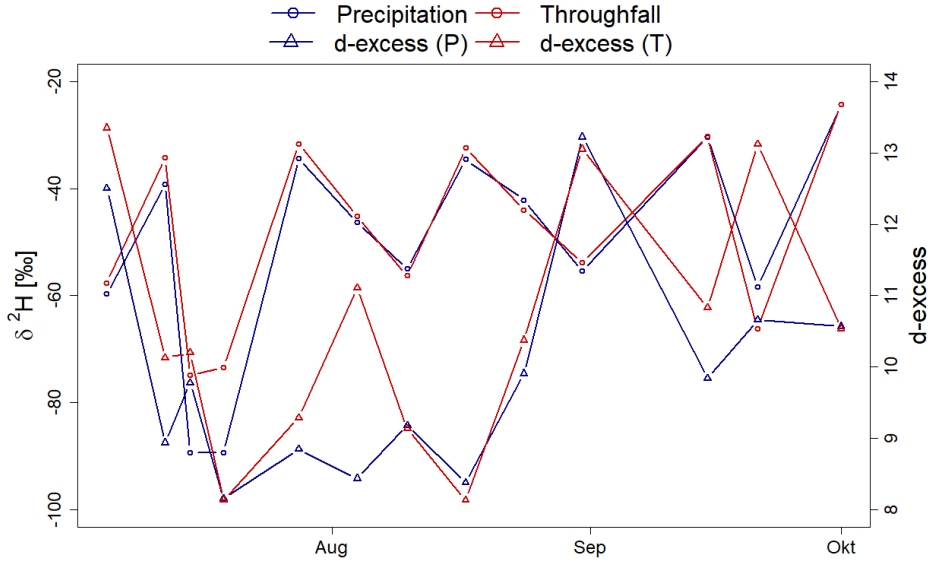

Figure 19: Temporal course of precipitation (blue) and throughfall (red) δ^2H values with corresponding d-excess. The lines between the measuring points (circles and rectangles) are interpolated

3.5.4 Spatial Variability

The results of an inversed distance weighted interpolation (IDW) of the measured δ^2H values of throughfall from 07.05.2021 is depicted in *Figure 20* in order to show the spatial variability at our study site. Therefore, we anaylzed the isotopic composition of the throughfall at each plot (in total: 27 samplers). The samplers were installed with an average distance of two meters to each other. The interpolation was calculated with an distance coefficients of 1 and intervals were set to >0.5 ‰ in order to meet the guaranteed precision of the used CRDS (L2120-, Picarro, Santa Barbara, USA) for isotope measurements in liquids. The values varied from -60.82 to -55.36 ‰ and were most positive between the beech stands (A,B,C).

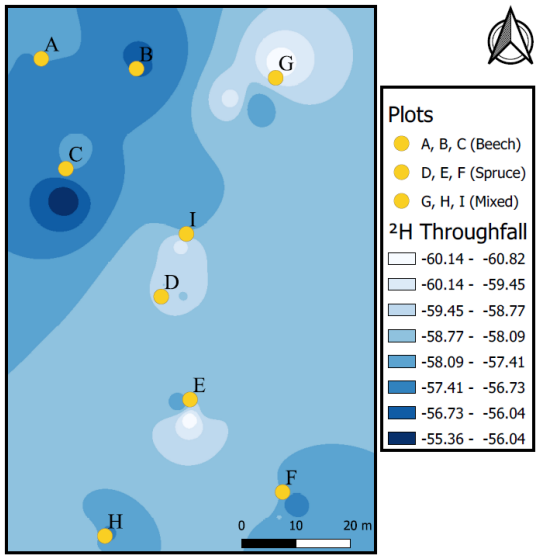

Figure 20: IDW interpolation of throughfall δ^2H values from 07.05.2021

Figure 21 shows the spatial variability of the effects of evaporation on soil water isotopes by showing the d-excess values of shallow soil water. We derived the d-excess values from the soil water δ^2H values in 5 and 20 cm soil depth and interpolated values between the plots. In general, the average d-excess values in 5 cm soil depth (5.21) were higher than in 20 cm soil depth (4.19). Showing the largest interpolated d-excess values in 5 cm soil depth from 5.39 to 8.32 between the plots B,C,D,E and I . The variability between the different plots decreased in the 20 cm soil depth, with for most cases, smaller d-excess values compared to the values in the upper soil layer. However, this is not true for plot A and E where we observed and interpolated higher d-excess values in the lower soil depth.

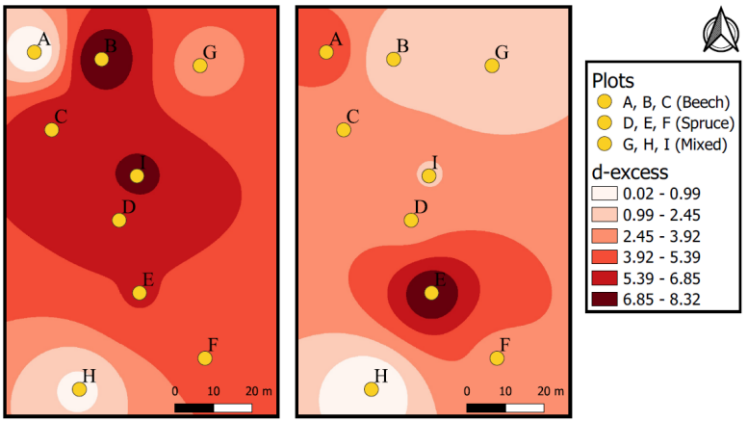

Figure 21: Spatial variability of IDW interpolated d-excess values at 5 and 20 cm soil depth. Derived from soil water δ^2H values from destructive sampling on 07.17.2021

The spatial variability of soil water δ^2H values (destructive values) is shown in *Figure 22* for soil depths of 5, 20, and 40 cm. We present the measured values from a wet and a dry period. The values between the plots are again IDW interpolated. δ^2H values observed on 07.16.2021 (wet period) were more positive compared to the values from 10.05.2021 (dry period). The results show a high spatial but also temporal variability between the plots and dates. In general, the δ^2H values from the wet period were more positive than the values of the dry period. The shallow soil water in 5 cm soil depth was more enriched in heavy isotopes and became more depleted in deeper soil depths for both periods. But the values differed strongly in their depth specific variability. The variability between plots was the lowest in 5 cm soil depth for the wet period and at 40 cm for the dry period. The highest variability for observed and interpolated values was in 40 cm depth for the wet period and in 5 cm for the dry period.

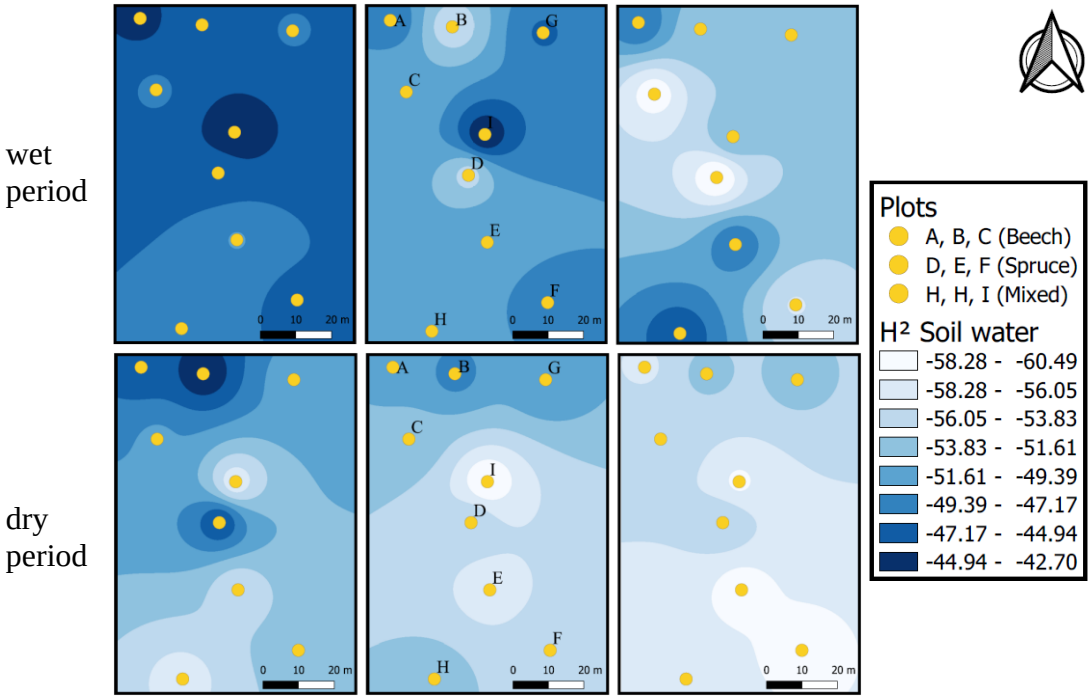

Figure 22: Spatial variability of IDW interpolated soil water δ^2H values at 5, 20 and 40 cm soil depth. Derived from soil water δ^2H values from destructive samplings 07.17.2021 (wet period) and 10.05.2021 (dry period)

3.5.5 Spatiotemporal Variability of Soil Water Isotopes

The temporal variability of soil water isotopes over a period of two weeks is depicted for plot I (mixed stand) in *Figure 23.* The time period can be divided into two wet periods (08.06-08.07.2021 and 08.16- 08.19.2021) and one dry period (08.08 – 08.15.08) which are highlighted by different background colors.

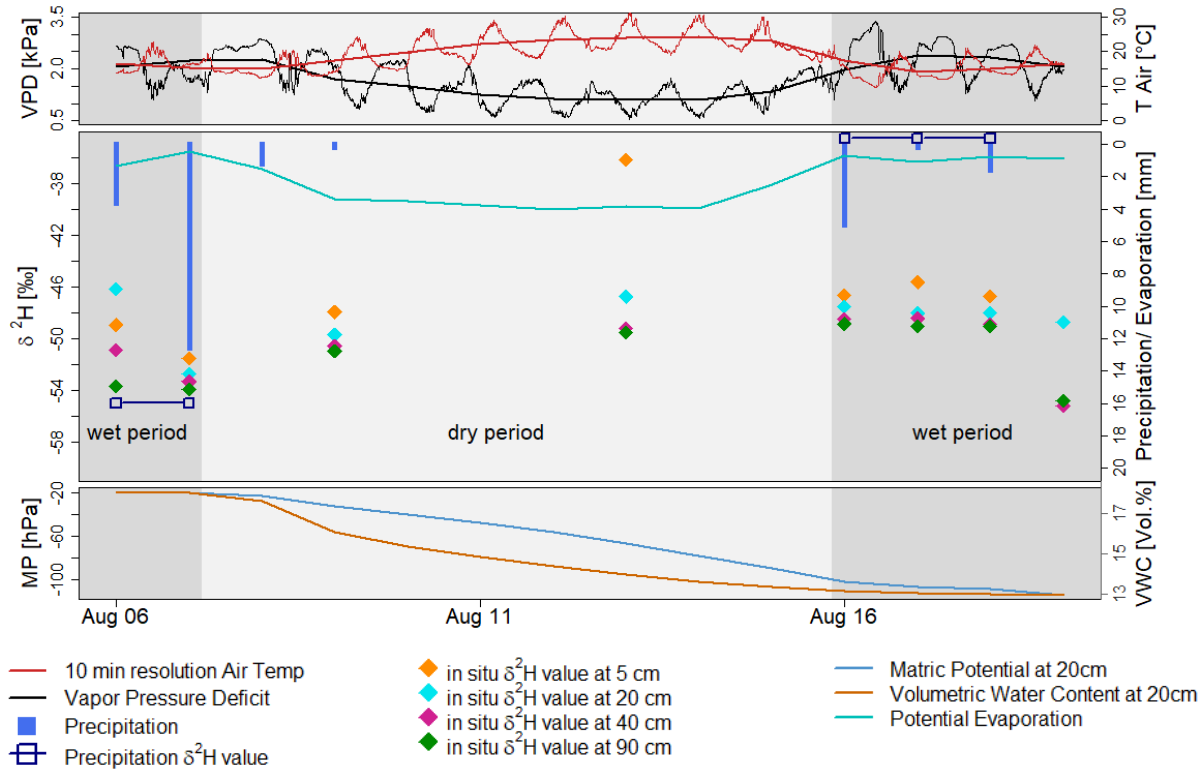

Figure 23: Temporal variability from 08.06-08.19.21 of soil water δ^2H values at 5, 20, 40 and 90 cm soil depth for plot I. In addition: Air Temperature (red lines) vapor pressure deficit (black lines) at different resolutions, potential daily evaporation (light blue line) and daily precipitation. Daily median of volumetric water content (dark orange line) and matric potential (blue line) at 20 cm soil depth and average δ^2H values of the precipitation events (dark blue squares)

The total precipitation amount during the first wet period was 15.2 mm and 6.8 mm during the second wet period respectively. The total precipitation amount during the dry period was 1.4 mm. During the dry season the daily average temperature increased from 15.14 °C at the beginning of the period to 24.36 °C on August 14th, while the vapor pressure deficit decreased analogously with 1.71 kPa at the beginning of the dry period and 1.09 kPa on August 14th. Matric potential and volumetric water content followed the same trend, with a plateau during wet periods while decreasing during the dry period. During the first wet period, the measured matric potential was on a peak with -19 hPa at 20 cm soil depth (-10 hPa at 40 cm) and decreased to -101 hPa (-73 hPa at 40 cm) at the end of the dry period. The volumetric water content was 18.07 Vol.% (31.11 Vol.% at 40 cm) at the beginning of the first wet period and decreased to 13.13 Vol.% (27.75 Vol.% at 40 cm) at the end of the dry period. Since the MP and VWC values of the 20 and 40 cm soil depths were close to each other, only the values at 20 cm soil depth are pictured for better clarity.

The δ^2H values of the soil water can be clearly distinguished between the different soil depths, and were decreasing with increasing depth. On August 06th, the δ^2H value at 5 cm

was -46.01 ± 92 ‰ and -53.66 ± 0.89 ‰ at 90 cm soil depth. The values became more negative during the first wet period (average precipiation δ^2H value of both events: -54.99‰), especially after the second and largest precipitation event on August 07th with a amount of 12.6 mm. Coinciding with the event, the δ^2H values of the individual depths moved significantly closer together from -51.54 ± 0.92‰ at 5 cm to -53.91 ± 0.82‰ at 90 cm. During the dry period, all δ^2H values increased, where the distance of the measured isotopes was the largest between the 5 cm depth (-36.16 ± 0.71‰) and the other depths, followed by the 20 cm layer (-46.76 ± 0.68‰). While the values in 40 and 90 cm soil depth were still close to each other with -49.21 ± 0.77‰ at 40 and -49.52 ± 0.80‰ at 90 cm respectively. The average precipiation δ^2H value of the second wet period was -42.13‰. The soil water δ^2H values decreased after the first precipitation event on August 16th, but then remained constant for 3 days until they dropped on August 19th. Whereas the values in 40 and 90 cm depth dropped strongly from -48.86 ± 0.88‰ to -55.19 ± 0.63‰ at 40 cm and from -49.02 ± 0.78‰ to -54.78 ± 0.71‰ at 90 cm soil depth.

Figure 23 shows that the soil water isotopes responded to precipitation events by changing values (either becoming heavier or lighter), but the precipitation and soil water δ^2H values differed significantly. *Figure 24* is intended to illustrate the extent to which the δ^2H values in soil water differed from those in precipitation. The Figure shows the in situ soil water δ^2H values in 5, 20, 40 and 90 cm soil depth of all plots over a period of three weeks. In addition, the volume-weighted weekly precipitation is shown, with the position of the bars corresponding to the isotopic signature and the magnitude corresponding to the amount of precipitation.

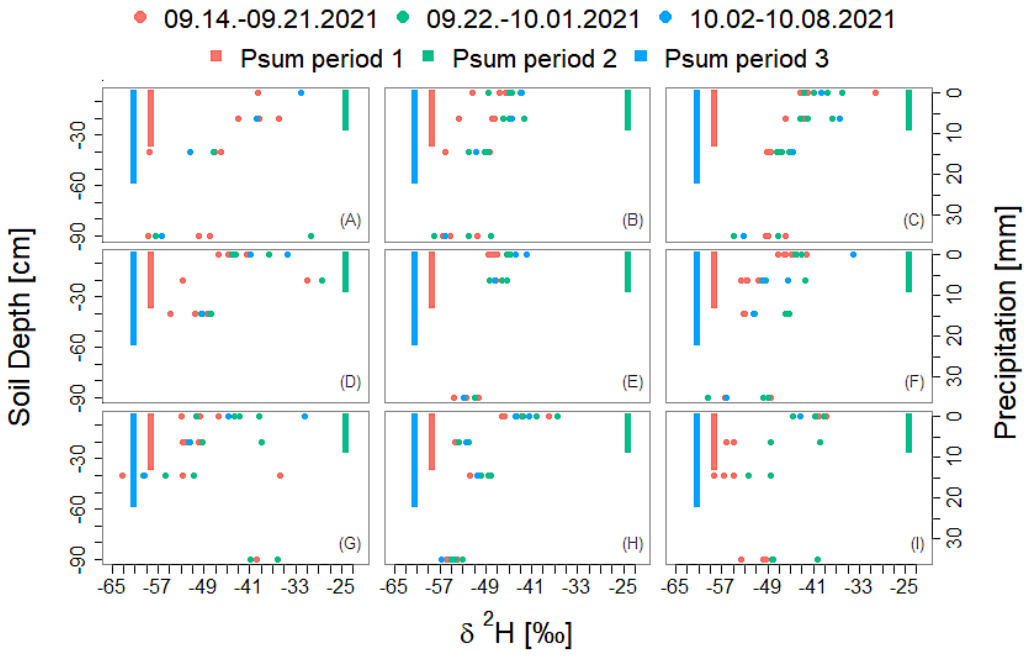

Figure 24: Soil water δ^2H values respond to precipitation events from 09.14- 10.02.21. Symbol color represents the time period of depicted data. Soil water δ^2H values and volume-weighted weekly precipitation with the position of the bars corresponding to the isotopic signature and the magnitude corresponding to the amount of precipitation

In general, the variability of soil water δ^2H values decreased with increasing depth and the δ^2H values of shallow soil water were more positive compared to deeper soil waters. The shown δ^2H values are located between the values of the precipitation events, but with strongly diverging distances.

The smallest distances between δ^2H values of soil and precipitation water were at plots A and I, where some δ^2H values corresponded very close (e.g. plot A in 40 cm : -56.28‰, precipitation: -58.36‰) to those values of the precipitation water of the corresponding week, in this case period 1. However, at other plots, e.g., C and E, the values differed strongly from each other. This was also the case for the other two periods, where the δ^2H values of soil and precipitation water differed strongly at all plots.

The precipitation events from periods 1 and 2 had a larger influence on the soil water isotopes than the events from period 2, which were significantly more negative, but formed less precipitation amount overall. Although this pattern can be observed at all plots, the degree to which it is observed differed between the plots. For example, the drift of the soil water δ^2H values in 90 cm depth to the precipitation values was larger at plot H with an average value of -54.31‰ than at plot I with an average value of -49.94 ‰ (considering matching number and times of measurements).

3.6 Variance Analysis

Based on the results shown in chapter 3.1 Soil Analysis, we formed the first main group "Groups by Soil" with two subgroups, one with all plots where the soil texture of the Ah and Bv horizons were silty loam and one with clay loam texture. The classification is shown in *Table 6.*

Table 6: Classification of "Group by Soil"

Plot	Stand	Subgroup by soil texture
A,B,C,I	3 × Beech 1 × Mixed	Silty loam
D, E, F, G, H	3 × Spruce 2 × Mixed	Clay loam

The classification of the second main group "Groups by Stand" resulted from the three tree stand types, Beech (plot A,B,C), Spruce (plot D,E,F) and Mixed (plot G,H,I).

Basis of the statistical evaluation were the isotope values from the destructive equilibration bag method. The tests were not performed separately for each sample date but with the data of all three measurements together in order to maximize the population size of each subgroup.

The cumulative distribution functions of the isotope values of each plot are presented in the Appendix in *Figure A.* 6 for δ^2H and in *Figure A.* 7 for $\delta^{18}O$ respectively. The application

of the Anderson Darling test also proved that the populations of each subgroup from "Group by Stand" were normally distributed. The null hypothesis that the populations are normally distributed was accepted ($p > 0.05$). This was the case for each subgroup and soil depth, respectively. A detailed presentation of the distributions and the results of the Anderson-Darling test is provided in the Appendix *Table A. 6* for the δ^2H values and in *Table A. 7* for the $\delta^{18}O$ values respectively. The standard deviations of the δ^2H values of the subgroups at each soil depth were equal and thus homogenous. The Levene's test yielded a non-significant result ($p > 0.05$) for the null hypothesis that the values are equal and was therefore accepted. The same applied to the subgroups of the other main group "Groups by Soil". The data thus met the requirements for ANOVA and two-sided t-test respectively.

For the "Group by Stand" the mean δ^2H values of each subgroup at the same soil depth varied, showing the most enriched values at the beech plots and the greatest depletion of heavy isotopes within the spruce plots. The largest deviation was in 5 cm soil depth, with a δ^2H value of -46.74 ± 0.78‰ for the beech plots, -50.13 ± 0.76‰ for the spruce and -49.86 ± 0.66‰ for the mixed plots. However, these differences were not significant, tested by ANOVA with the null hypothesis that the values originate from the same population being accepted ($p > 0.05$, $n = 27$). This was true for all soil depths of main group "Groups by Stand" for both, δ^2H and $\delta^{18}O$ values. The results of the Levene's test and ANOVA are shown in the Appendix in *Table A. 8* for the δ^2H values and in *Table A. 9* for the $\delta^{18}O$ values respectively.

No significant differences were found between the two subgroups of the second group of interest "Groups by soil" either, this applied to all three soil depths. The null hypothesis that the soil water isotope values of both subgroups at each soil depth originate from the same population was accepted ($p > 0.05$, $n = 41$). The same was true for the isotope values of all soil depths combined ($p > 0.05$, $n = 81$). The results of the Levene's test and two-sided t-test on "Groups by Soil" are shown in the Appendix in *Table A. 10* for the δ^2H values and in *Table A. 11* for the $\delta^{18}O$ values respectively.

3.7 Regression Model

The basis of the GLM were the in situ δ^2H values as the dependent, responce variable. $\delta^{18}O$ values were excluded because of their implausibility. Choosen independent (predictor) variables were precipitation, C/N ratio, volumetric water content, matric potential, soil temperature, CEC and pH.

The predictor variables and residuals were tested for collinearity and homoscedasticity. The variance inflation factor of the matric potential and volumetric water content was larger than 10, thus the variables were collinnerar. They highly correlated with a spearman correlation factor of $p < 0.01$. For this reason, we excluded the matric potential values from the GLM, as the volumetric water content data was more frequently available.

The results of the GLM are presented in the Appendix at *Table A. 12*, showing a highly significant result ($p < 0.01$) but a poor model performance with an adjusted R^2 of 0.32. The independent variables that had an impact on δ^2H ($p < 0.05$) were precipitation, soil temperature, C/N and pH. The precipitation values were the values of the previous day (- 1

day). There was no significant impact ($p > 0.05$) of the precipitation on δ^2H values at matching days. The impact of precipitation from two previous days (- 2 days) was smaller than the impact of precipitation of the previous day (- one day) with $0.05 > p > 0.01$.

By exluding the predictor C/N, the adjusted R^2 reduced to 0.28 (with same p-value), but the previous non significant predictors Ca, Mg and K turned highly significant ($p < 0.001$). A detailed presentation of the results is shown in *Table A. 13* in the Appendix.

4. Discussion

In the following chapter, key findings of this research are discussed and reviewed. The chapter is structured according to the methods and results sections, but also partly overlaps topics.

4.1 Soil Properties Analysis

The criteria why we choose this study site in Ettenheim was, that we were expecting homogenous soil conditions, power supply as well as a suitable distribution of beech, spruce and mixed stands. Brown soils on sandstone are very variable soils in terms of their appearance, skeleton heterogeneity and physicochemical properties (GeoLa, 2021). But due to the relatively small research area of 0.75 ha we were hoping to meet similar soil conditions between the stands. The soil texture analysis by finger test revealed that most of the analyzed horizons can be grouped into soil textures of clay loam or silty loam. But this method is very inaccurate and error prone. The sedimentation and sieving method would have been a more accurate choice, enabling a clear differentiation of sand, silt and clay contents at all horizons.

The pH values were all in the range between 4.48 and 5.31 and therefore generally acidic, which is typical for brown soils on sandstone (Amelung et al., 2018). The analysis revealed that there was no pattern of pH between different soil depths. But the results show that the soils under the spruce trees were the most acidic, followed by the mixed stands. These results are consistent with other studies e.g. (Genssler, 1959; Nihlgård, 1971) and are caused by acidic substances such as polyphenol in the litter of spruce trees which lead to acid-forming humus.

When comparing the different stands, we did not detect a pattern in the distribution of exchangeable cations. All values decreased with increasing soil depth as expected, since mineralization processes are more pronounced in the humus-rich and well-aerated upper soil layers. Gensler (1959) and Nihlgård (1971) found lower K^+, Ca^{2+} and Mg^{2+} concentrations in soils of spruce stands compared to beech stands, whereas we did not. However, because we performed the CEC analysis for only three plots (each representing a stand type), this number is insufficient for an evaluative comparison.

In general, the C/N ratios decreased with increasing soil depth suggesting a lower carbon content in deeper, humus-poor soil layers. Our results ranged from ratios of 15.12 to 24.71 in the upper soil layers and thus seem plausible for soils under beech and spruce stands compared to the findings of other studies (Albers et al., 2004; Cremer et al., 2016; Fabiánek et al., 2009), although our ratios are somewhat lower. The lower values might be due to the time of sampling. We took the soil samples in April at the beginning of the vegetative phase.

Due to the climatic conditions in our region and the elevated location, little mineralization of the litter from the previous year can be expected because of the low temperatures. Sampling later in the vegetative phase could have resulted in higher C/N ratios as the previous year's litter gradually decomposes and nitrogen removal increases due to plant growth.

We did find significant lower total nitrogen concentrations in the upper 5 cm layer of the spruce stands compared to the beech stands. In 5 cm we measured an average total N content of 0.13 (ton ha^{-1}) at the spruce stands and an average N content of 0.16 (ton ha^{-1}) in the soils under the beech stands. The averaged total carbon contents were similar with 2.85 (ton ha^{-1}) for the spruce and 2.77 (ton ha^{-1}) at the beech stands. Resulting in lower C/N ratios in the soils of the spruce stands compared to the beech stands in the most upper soil layer. These results are consistent with those of others e.g. (Cremer et al., 2016; Genssler, 1959) and may be due to a higher mass of microorganisms in soils under beeches leading to increased N mineralization (Bagherzadeh Chaharjouee, 2004).

4.2 Soil Water Retention Characteristics

The evaluation of meteorological data showed that we observed a relatively variable summer, which was humid and mild compared to the dry and hot years before. The wettest period was in July and from then on it became progressively drier until the end of the measurement campaign. These observations are also reflected in the soils.

Volumetric water content and matric potential followed the same trend with decreasing values after August, and thus is consistent with our recorded meteorological data. But the values differed among the different plots strongly in terms of magnitude, indicating high heterogeneity of the soils with divergent water retention characteristics. This heterogeneity exists even for different layers at the same plot as we showed in *Figure 12*, where we measured lower matric potentials at plot E & F in 40 cm than in the 20 cm layer above, although the water content increased in deeper layers.

We measured the lowest variability of VWC in the soils under the mixed plots, independent of the predominant soil texture (plot G and H = clay loam, I = silty loam). And at 90 cm soil depth, the lowest values were measured in the soils of all three mixed plots. These patterns of the measured VWC values at the mixed plots might be due to different rooting depth and more dense distribution of fine roots as well as increasing transpiration rates of beech trees under competition which would be in accordance with the findings of others (Bolte & Villanueva, 2006; Schmid, 2002; Schume et al., 2004). A steep and rapid increase in VWC after precipitation events was observed at plots B, D, and E in 40 cm and at plots A and E in 90 cm, indicating either preferential flow or, more likely, stagnation of water in these layers or at least near the installed sensors.

The comparison of the MP sensor types (T8 and MPS-2) clearly demonstrated the expected higher sensitivity of the T8 sensors (Decagon Devices Inc, 2011; Solutions, 2017). For this reason, we decided to use the values from the T8 in order to model the SWRC expecting to achieve better model fit which indeed was the case. The positions of our modelled SWRC's were all within the range of sandy loam and clay loam textures from the

literature. The shape of our modeled SWRC's did most closely resemble that of the sandy loam except for plots C and H, which showed more of the SWRC shape of clay to silty loam.

The observed variability of our model performances could be since the soil layers did not settle completely after the VWC and MP sensors were installed. This may have created cavities around the sensors where water accumulated. Other reasons such as preferential flow could lead to differently pronounced readings from the VWC and MP sensors, distorting the correlation and resulting in poor model performance. However, we wanted to prevent this as much as possible by computing the model using the median values of VWC and MP instead of the mean values.

Our modeled SWRC's differ somewhat from the results of the soil texture analysis by finger test. We would have expected at least similar van Genuchten parameters for plots A, C, and I (soil texture analysis: silty loam) and for plots E, F, and H (soil texture analysis: clay loam), regardless of how they compare with the values derived from the literature. The position and expression of our modeled SWRC's again indicate the high heterogeneity of our investigated soils and indicate other factors besides soil texture e.g., cavities, skeleton fraction and preferential flow that influence soil water infiltration and distribution patterns.

We tried to compare our model results with those from the literature. However, these derived values were mostly obtained under laboratory conditions, whereas our values were obtained under natural conditions in very heterogeneous soils. Moreover, for this reason our values were limited to relatively small ranges (for VWC around 10 Vol.% and for MP from -850 to 0 hPa). Therefore, we might have obtained different results if we had covered a higher variability of soil moisture and matric potential values. Finally, the modelled results of the soil water retention characteristics, both from literature and from us, should not be weighted too heavily since the van Genuchten equation is empirical based and the results can be affected by environmental influences under natural conditions.

4.3 Soil Water Isotopes

In the following chapter, we evaluate our results on isotope measurements of both applied methods. First, we process the results of the equilibration bag method, which we also use to account for the spatial variability of our soil water isotope measurements. We then compare the results of our two methods and discuss in detail some of the findings obtained from the in situ measurements.

4.3.1 Equilibration Bag Method, Precipitation and Throughfall

In *Figure 14* we show that most δ^2H values measured with the equilibration bag method follow a similar trend. The values in the upper 5 cm soil depth were more enriched in the heavy isotopes and become more depleted with increasing depth. This observation is reflected in all our figures indicating isotopic fractionation by evaporation in the upper soil layers.

While we found no significant differences in the standard deviations, the soil water isotope values differed among the stand types. We measured the most negative δ^2H values in the soil water under the spruce plots and the most positive under the beech plots. However,

this was not true for the $\delta^{18}O$ values. The deviation of the $\delta^{2}H$ and $\delta^{18}O$ values could be related to an unevenly distributed isotope fractionation of soil water by evaporation. This is quite to be expected in a dense forest where the soil is exposed to sunlight to varying degrees.

Our results from chapter 3.5.4 Spatial Variability highlight this assumption. *Figure 21* shows the deviating d-excess values of the shallow soil water. And *Figure 20* shows that the $\delta^{2}H$ values in throughfall were most positive at the beech stands which could be due to a higher LAI of beeches and thus longer water retention by the foliage. Yet, the interpolated values between the plots should not be weighted in these figures. The chosen method (IDW) is not the most accurate (Yang & Xing, 2021) and the distances between our measurements were probably too high for interpolation. We also tried the more valuable kriging method, but it resulted in a poorer model performance (RSE of 3.55) compared to the IDW interpolation with a RSE of 3.21 (model parameters were optimized by Geostatistical Wizard, ArcGIS Pro).

In general, the measurements from the destructive method showed no temporal trend such as we have seen from the VWC and MP in chapter 3.3 Volumetric Water Content and Matric Potential.The isotope values were highly variable between sampling dates such as the isotope values we obtained from throughfall and precipitation (see *Figure 19*). Where we again, found very high variability and no trend, although we would have expected the isotopic composition of events to be more enriched in heavy isotopes in the hot summer months and more depleted in the colder months due to kinetic fractionation (Van der Straaten & Mook, 1983).

Most of the throughfall samples were more enriched in heavy isotopes than the precipitation samples. This was to be expected, as the throughfall is exposed to the atmosphere for a longer period due to water retention by the foliage and thus fractionation processes by evaporation. However, in some cases we obtained higher d-excess values in the precipitation samples than in the throughfall samples. This might be due to the distance of 500 m between the throughfall samplers and the climate station (this distance was necessary to find an exposed site in the forest). This could lead to spatial deviation of precipitation, which we did not consider with our set up. In addition, we cannot exclude the possibility that the precipitation collector was exposed to direct sunlight at times, which could have distorted the isotopic composition. After all, our soil water isotope values measured with the equilibration bag method as well as the precipitation and throughfall values fit well to the GMWL ($\delta^{2}H = 8\ \delta^{18}O + 10‰$) and LMWL ($\delta^{2}H = 7.56\ \delta^{18}O + 3.83‰$) as shown in a dual isotope plot (see *Figure A. 8*). Note that we derived the LMWL from precipitation data collected over several years at the University of Freiburg. Due to the distance of approximately 40 km, the LMWL cannot be taken directly for our location. Anyhow, it serves as orientation, since our measurement series did not contain sufficient data.

4.3.2 In Situ Isotope Measurements

Figure 16 gives an overview of all isotope values measured in situ and illustrates that our data series are sometimes very incomplete. We were only able to measure at a few plots and depths over the entire period, and there were hardly any days on which all probes delivered

correct values in succession. This was partly due to the high number of connected probes, which reduced the measurement frequency. The main reason however was the mild and humid summer that led to unexpectedly high soil water contents compared to previous years. This significantly delayed progress on the installation of the probes. On the other hand, the high water contents in the soils meant that we were often unable to flush the probes enough before the next measurement cycle began. In addition, we reconnected the gas transport lines of the probes under the spruce plots incorrectly after maintenance in August, which led to the fact that we had to discard the measured values of that period. Some probes failed due to liquid water that penetrated the membrane head to an extend that we were not able to flush them dry. Finally, our CRDS was down for several days in October.

In *Figure 17* we compare the measured δ^2H values from both methods on 08.17.2021 (± one day in case of the in situ values). There were no significant differences of the measured values except for plot A standing out. This was expected as both methods rely on the same principle thus measuring the same (mobile) water pool. Our results are consistent with the findings of (Volkmann & Weiler, 2014) when comparing the performance of both methods. Another but less time accurate comparison of the results from both methods can be seen in *Figure 18*.

Here we show boxplots of the in situ measured δ^2H values for each soil depth and month, separated by stand type. In addition, the values from the equilibration bag method were added. This figure is not well suited for the performance comparison of both methods, since the in situ and bag measurements do not always overlap temporally. E.g., for July, where only few in situ values were available (in the case of spruce and mixed stands the first measurements started at the end of July, while destructive was sampled on 07.16.21, same for October, Picarro failed during the destructive sampling time ± 4 days). But still, most of the destructive measured values were within the quantile range of the in situ values.

The figure shows that the values of both methods varied across all months and soil depths, as we have already observed in *Figure 14*. This behavior is again reflecting the high variability of the isotopic composition of precipitation and throughfall (see *Figure 19*).
Further, the in situ measured δ^2H values in 5 and 20 cm soil depth became more positive over the time, while the values in 40 and 90 cm were more stable. The lowest observed variability of all stand types was in September which was the driest month of the measurement campaign, as shown in *Figure 9, Figure 10* and *Figure 12*. These findings demonstrate that the variability of soil isotopes is strongly dependent on precipitation.

In most months, the variability of δ^2H in soil water was highest under the mixed stands in 40 and 90 cm soil depth (except for October, but this was due to missing data as described above). In addition, δ^2H values were most negative under the mixed plots at all soil depths. The higher variability of δ^2H under the mixed stands in 40 and 90 cm soil depth might be related to fast infiltrating water from precipitation through preferential flow. Which, in turn, could be more present in the mixed stands due to a shift to deeper rooting of beech under competition as described in chapter 4.2 Soil Water Retention Characteristics The deeper rooting could also be an explanation of the generally more negative values in the soil water under the mixed stands. Isotopically depleted water from deep soil layers could be redistributed to upper layers via the plant root system and mycorrhizal networks.

The higher δ^2H values in the upper soil layers indicate isotopic fractionation of the shallow surface soil water by evaporation. This assumption is reinforced by the positive trend over the months. Which is accompanied by the decreasing VWC and MP values from *Figure 10* and *Figure 12* indicating little mixing of shallow soil water with precipitation and throughfall. In the deeper layers of 40 and 90 cm the mean values did not show a trend and the quantiles were more stable, which indicates that the isotopic fractionation by evaporation was less or not present at all.

4.3.3 Detailed View on Spatiotemporal Dynamics of Soil Water δ^2H Values

In *Figure 23* we show a detailed overview of the temporal dynamics of the in situ measured soil water δ^2H values at plot I (mixed stand) for a period of 2 weeks. The results presented on this figure combine some of the observations already mentioned in one figure and are intended to reinforce our statements. The δ^2H values increased significantly at all soil depths during the dry period which can be related to the increasing evaporation rate. Interestingly, even the values in 40 and 90 cm soil depth seem to be affected as they increased although significantly less than the values in the upper layers. The order of magnitude in which the values increased show the extent to which the soil water in the individual layers was affected by evaporation.

At the beginning of the first wet period, the δ^2H values at each soil depth were clearly distinguishable, but after the second precipitation event, the values merged close to the δ^2H value of the precipitation event. This indicates almost complete mixing of water between all layers. Even though the VWC and MP were on a peak, these observations indicate that the older mobile water was displaced and that the soil water in all layers mixed homogeneously with the precipitation water as assumed by the translatory flow (Hewlett, 1982; Horton & Hawkins, 1965). The average δ^2H value of the precipitation from the second wet period was significantly more positive than from the first period. This again highlights the high variability of δ^2H values we observed in precipitation and throughfall. However, this time the isotope signature of the precipitation was not reflected in the soil water. The δ^2H values of the soil water decreased drastically after the first event. Thereafter, they remained relatively constant until they dropped drastically again on the last day of the period, although no precipitation fell on this day.

Again, infiltration processes seem to strongly influence the isotopic composition of the soil water. This time, however, the change was much more delayed than during the first wet period. This may be due to the significantly lower precipitation amount. But it does not explain why the δ^2H values of the soil water dropped significantly on the last day. The measured δ^2H values in the soil water are in contrast with those we measured in the precipitation during both wet periods. Either even older water was mobilized, or the layers were influenced by subsurface or groundwater flow. In contrast, VWC and MP values remained relatively constant during the second wet period, indicating that the groundwater table did not rise. At a depth of 70 to 90 cm directly above the sandstone layer, we found high clay contents in most of the plots. These high clay contents could form a poorly permeable layer that could lead to subsurface flow in our slope situation.

The origin of the strongly depleted water remains unclear, since we measured close to the highest point of the mountain. These observations highlight the advantages of stable water isotopes as natural tracers as well as the possibilities with isotope measurements of high temporal resolution.

The results from *Figure 23* were collected during a comparatively wet period. They show that δ^2H values in soil water mixed with those of precipitation more rapidly under moist soil conditions than under dry soil conditions with lower MP and VWC.

To examine this behavior in more detail, *Figure 24* shows the difference between soil water and precipitation δ^2H values during a comparatively dry period. The measured δ^2H values in precipitation and soil water differed considerably. A complete mixing of precipitation and soil water cannot be assumed here based on the isotopic composition. The δ^2H values of both water sources from the first period were most similar (this was also the week with the highest measured VWC and MP values). Although the amount of precipitation in the third period was twice as high with a similar composition, the δ^2H values in the soil water deviated strongly from those in the precipitation. A possible explanation for this could be that most of the precipitation ran off by surface runoff or infiltrated by preferential flow without mixing with the soil water in the desiccated soil matrix.

4.4 Variance Analysis

In order to test the impact of different soil textures and stand types on the soil water isotopes, we analyzed the variances of the measured isotopes to check for differences between of our plots. Therefore, we divided the soil water δ^2H and $\delta^{18}O$ values of all plots into subgroups of two main groups, “Group by Soil” and “Group by Stand”. Our null hypothesis was, that the values of the subgroups originate from the same population. The null hypothesis was accepted for both main groups with a result of ($p > 0.05$, $n = 27$) for “Group by Stand” and ($p > 0.05$, $n = 81$) for “Group by Soil”. This was true for all four soil depths and both isotopes respectively.

However, the three destructive samplings provided only little data and the observed values by this method were highly variable as our results show in *Figure 15* when comparing values from the same date.

This could be since it could not be avoided that the soil samples were taken at deviating sampling depths. Further, samples from different dates were taken at slightly different locations. In addition, it could not be ruled out that soil layers mix with each other when taking the soil sample. Our results have highlighted the high spatial variability of soil water isotopes and therefore question the suitability of the destructive method for comparing results from different samples. By using the in situ method, we hoped to avoid these problems. Nevertheless, we decided to use the measurements from the equilibration bag method for the variance analysis because the in situ values did not match sufficiently in time.

But the in situ results depicted on *Figure 18* show that at least visually a difference can be seen between different stand types. The same is true in case of the different soil types, as shown in *Figure A. 9* in the Appendix.

For this reason, we analyzed the variances of the in situ values as well but conditionally. By testing the same null hypothesis as above, we did not find significant differences ($p >$

0.05) of δ^2H values between the plots in the subgroups silty loam and clay loam at 5 cm soil depth. But we did find highly significant differences in the other layers ($p< 0.01$). In case of the "Group by Stand", we did not find significant differences between the pure beech and spruce stands ($p> 0.05$) at 5, 40 and 90 cm soil depth. But we found highly significant differences of the soil water δ^2H values between the beech and mixed stands as well as between the spruce and mixed stands ($p< 0.01$) at all soil depths. Since the distribution of most in situ values was found to be non-normally distributed (see distribution histograms *Figure A. 10* and *Figure A. 11*) and the variances within the subgroups were mostly heterogeneous, we resorted to the methods described in chapter 2.5.3 Variance Analysis

The differences between the subgroups by soil texture could be linked to the different pore size distribution and thus deviating equilibrium fractionation of soil water (Gaj & McDonnell, 2019; Orlowski & Breuer, 2020). This could also explain why δ^2H values did not differ in the 5 cm layer, as this layer consists mainly of humus at each plot.

We did not find significant differences of the δ^2H values between the pure beech and spruce stands at most soil depths. But we found significant differences between the δ^2H values in the soil water under the beech and mixed and the spruce and mixed stands in each soil depth. This could indicate deeper rooting of beech under competition. Which in turn could lead to preferential flow and hydraulic redistribution. These findings would fit to our previous observations from chapter 4.2 Soil Water Retention Characteristics. However, these findings are conditionally.

4.5 Regression Model

The results of the linear regression from chapter 3.7 Regression Model show that our measured soil water δ^2H values depended on precipitation, soil temperature, C/N, and pH.

However, we obtained a poor model performance with an adjusted R^2 of 0.32. This shows that almost 70% of the δ^2H variance cannot yet be explained by our predictor variables which were based on physiochemical soil properties, even by extending the model with daily precipitation. This indicates that there are still many factors influencing soil water ^2H that we have not accounted for in our approach. Such factors may include the volume and isotopic signature of groundwater and subsurface flow, precipitation and throughfall, or factors affecting the isotopic fractionation such as evaporation or soil texture.

If we had used a more accurate method to determine the soil texture (e.g. sedimentation method), it would have been interesting to include the percentage of silt, clay, and sand in the regression model. We did not measure the isotopic composition of the groundwater or the subsurface flow. The resolution of our precipitation and throughfall isotope measurements were too low, to be included in the model. The extension of the model with the daily evaporation rate showed neither a significant influence on the δ^2H values nor a significant improvement of the model performance. Similar to the precipitation approach, we tested the effect of evaporation on the δ^2H values from the following days but without significant results, not even in the shallow 5 cm soil layer.

By excluding the C/N ratio from the model, the adj. R^2 reduced to 0.28 but the previous non significant predictors Ca^{2+}, Mg^{2+} and K^+ turned highly significant ($p< 0.001$), see *Table A. 13* in the Appendix for a detailed presentation of the results.

Since the two predictors VWC and MP proofed to be collinear, we excluded MP from the model. Integrating MP instead of VWC, improved the model performance to an adj. R^2 of 0.35 with MP being highly significant ($p < 0.001$). In this process Al^{3+} became significant as well ($p < 0.05$). Since we installed the T8 MP sensors only in 20 and 40 cm soil depth, the values from the 5 and 90 cm layers were excluded from this approach. With the same reduced group size but VWC instead of MP, we reached a significantly lower model performance (R^2 of 0.29), but VWC became significant ($p > 0.05$). In addition, Ca^{2+} and Fe^{3+} became also significant ($p < 0.05$).

Changing the predictors in our GLM strongly affects the model outcome and performance. Which further highlights that many factors are still not considered in our approach. This becomes especially visible by the implementation of a dummy variable into the model. By the extension of our first model (R^2 of 0.32 and VWC instead of MP) with the current date as a factor, we have significantly improved the model performance (adj. R^2 of 0.59) which is a very good model performance. This also caused the predictors date (dummy), Na^+ and VWC to become significant ($p < 0.05$), whereas the previously significant variables soil temperature and precipitation were no longer significant. The results are shown in the Appendix in *Table A. 14*.

5. Conclusion and Outlook

We provide a detailed overview of the soil properties of our research area. We show that the water retention characteristics of our investigated soils are very heterogeneous among the different plots and soil depths. The methods we chose to analyze soil water isotopes show similar results. But we show clear advantages of the high-resolution isotope measurements with the in situ method over the destructive equilibration bag method. We provide insights into the high temporal variability of the isotopic composition of precipitation and throughfall and distinctly demonstrate isotopic fractionation of soil water by evaporation.

To answer our hypotheses, we relied on graphical representations and statistical analysis of our measurements.

Our first hypothesis was:

1. Different physiochemical soil properties affect the stable water isotope composition. (Soil texture, pH, C/N ratio, CEC, soil temperature, volumetric water content and matric potential)

We were not able to detect a significant difference in soil water isotopes with respect to the different soil textures. However, we did find significant dependencies of soil water ^2H and pH, C/N ratio, most cations, soil temperature, volumetric water content and matric potential. But our results from the regression model show that there are still many factors affecting the observed variance of ^2H in soil water that we did not consider in our approach. Furthermore, we show that with changing predictors (e.g., adding precipitation or excluding C/N) the significances change, which calls the statement of our model into question. Only the predictor variable matric potential was consistently significant across all model scenarios. Due to their implausibility, we could not apply the model for ^{18}O, which could have somewhat validated our results if the results were consistent.

Our second hypothesis was:

2. Different forest stand compositions have an impact on the soil water infiltration and distribution patterns.
   (Impact of RWU, rooting depth and distribution on infiltration patterns)

We did not detect significant differences in the isotopic composition of soil water among the different stand types, neither for ^{2}H nor for ^{18}O. By graphing the in situ data, we were able to visually highlight differences of soil water $\delta^{2}H$ values between stand types. However, we could not test these differences for significance because data availability was too inconsistent over time.

Our findings would improve if we considered not only physicochemical soil properties but also groundwater and subsurface flow in our regression model. Further our set up would enhance if we implement in situ measurements for precipitation and throughfall and do a detailed analysis of the soil texture e.g., with sedimentation method. Labeling experiments with water of known isotopic composition could strengthen our hypothesis of preferential flow and hydraulic redistribution by deeper rooting of beech under competitive conditions. The soil water isotope values that we measured could be recovered in the isotopic composition of xylem water and thus contribute to the study of water uptake strategies of individual tree species and their adaptation to different climate change scenarios.

We conclude high potential of holistic interdisciplinary studies among hydrologist, soil ecologists and plant physiologists. Finally, further data acquisition is needed to improve our conclusions. This, in turn, underscores the benefits of studies over longer time periods, as this may be the only way to adequately understand changes in forest ecosystems.

Bibliography

Albers, D., Migge, S., Schaefer, M., & Scheu, S. (2004). Decomposition of beech leaves (Fagus sylvatica) and spruce needles (Picea abies) in pure and mixed stands of beech and spruce. *Soil Biology and Biochemistry*, *36*(1), 155–164.

Allen, R. G., Smith, M., Pereira, L. S., & Perrier, A. (1994). An update for the calculation of reference evapotranspiration. *ICID Bulletin*, *43*(2), 35–92.

Allen, S. T., Keim, R. F., & McDonnell, J. J. (2015). Spatial patterns of throughfall isotopic composition at the event and seasonal timescales. *Journal of Hydrology*, *522*, 58–66. https://doi.org/10.1016/j.jhydrol.2014.12.029

Amelung, W., Blume, H.-P., Fleige, H., Horn, R., Kandeler, E., Kögel-Knabner, I., Kretzschmar, R., Stahr, K., & Wilke, B.-M. (2018). Scheffer/Schachtschabel Lehrbuch der Bodenkunde. In *Scheffer/Schachtschabel Lehrbuch der Bodenkunde*. Springer Berlin Heidelberg. https://doi.org/10.1007/978-3-662-55871-3

Bagherzadeh Chaharjouee, A. (2004). *Mechanisms of Carbon and Nitrogen transformations in Forest floors of Beech-, Spruce-and Mixed Beech-Spruce Stands*.

Berry, Z. C., Evaristo, J., Moore, G., Poca, M., Steppe, K., Verrot, L., Asbjornsen, H., Borma, L. S., Bretfeld, M., & Hervé-Fernández, P. (2018). The two water worlds hypothesis: Addressing multiple working hypotheses and proposing a way forward. *Ecohydrology*, *11*(3), e1843.

Beyer, M., & Dubbert, M. (2019). X Water Worlds and how to investigate them: A review and future perspective on <i>in situ</i> measurements of water stable isotopes in soils and plants. *Hydrology and Earth System Sciences Discussions*, *November*, 1–35. https://doi.org/10.5194/hess-2019-600

Bolte, A., & Villanueva, I. (2006). Interspecific competition impacts on the morphology and distribution of fine roots in European beech (fagus sylvatica L.) and Norway spruce (picea abies (L.) karst.). *European Journal of Forest Research*, *125*(1), 15–26. https://doi.org/10.1007/s10342-005-0075-5

Bowers, W. H., Mercer, J. J., Pleasants, M. S., & Williams, D. G. (2020). A combination of soil water extraction methods quantifies the isotopic mixing of waters held at separate tensions in soil. *Hydrology and Earth System Sciences*, *24*(8), 4045–4060. https://doi.org/10.5194/hess-24-4045-2020

Brinkmann, N., Seeger, S., Weiler, M., Buchmann, N., Eugster, W., & Kahmen, A. (2018). Employing stable isotopes to determine the residence times of soil water and the temporal origin of water taken up by Fagus sylvatica and Picea abies in a temperate forest. *New Phytologist*, *219*(4), 1300–1313. https://doi.org/10.1111/nph.15255

Brooks, J. R., Barnard, H. R., Coulombe, R., & McDonnell, J. J. (2010). Ecohydrologic separation of water between trees and streams in a Mediterranean climate. *Nature Geoscience*, *3*(2), 100–104.

Craig, H. (1961a). Isotopic variations in meteoric waters. *Science*, *133*(3465), 1702–1703.

Craig, H. (1961b). Standard for reporting concentrations of deuterium and oxygen-18 in natural waters. *Science*, *133*(3467), 1833–1834.

Cremer, M., Kern, N. V., & Prietzel, J. (2016). Soil organic carbon and nitrogen stocks under pure and mixed stands of European beech, Douglas fir and Norway spruce. *Forest Ecology and Management*, *367*, 30–40.

Dansgaard, W. (1964). Stable isotopes in precipitation. *Tellus*, *16*(4), 436–468.

Dawson, T. E., & Ehleringer, J. R. (1991). Streamside trees that do not use stream water. *Nature*, *350*(6316), 335–337.

Decagon Devices. (2008). *ECH2O-TE/EC-TM Water Content, EC and Temperature Sensors Operator's Manual*. 1–38.

Decagon Devices Inc. (2011). *Dielectric Water Potential Sensor Operator's Manual, Version 1*.

Demand, D., Blume, T., & Weiler, M. (2019). Spatio-temporal relevance and controls of preferential flow at the landscape scale. *Hydrology and Earth System Sciences*, *23*(11), 4869–4889. https://doi.org/10.5194/hess-23-4869-2019

Dubbert, M., & Werner, C. (2019). Water fluxes mediated by vegetation: emerging isotopic insights at the soil and atmosphere interfaces. *The New Phytologist*, *221*(4), 1754–1763. https://doi.org/10.1111/nph.15547

Evaristo, J., Jasechko, S., & McDonnell, J. J. (2015). Global separation of plant transpiration from groundwater and streamflow. *Nature*, *525*(7567), 91–94.

Fabiánek, T., Menšík, L., Tomášková, I., & Kulhavý, J. (2009). Effects of spruce, beech and mixed commercial stand on humus conditions of forest soils. *Journal of Forest Science*, *55*(3), 119–126.

Figueroa-Johnson, M. A., Tindall, J. A., & Friedel, M. (2007). A comparison of 18Oδ composition of water extracted from suction lysimeters, centrifugation, and azeotropic distillation. *Water, Air, and Soil Pollution*, *184*(1–4), 63–75. https://doi.org/10.1007/s11270-007-9399-8

Friedman, I. (1953). Deuterium content of natural waters and other substances. *Geochimica et Cosmochimica Acta*, *4*(1–2), 89–103.

Gaj, M., Beyer, M., Koeniger, P., Wanke, H., Hamutoko, J., & Himmelsbach, T. (2016). In situ unsaturated zone water stable isotope (2H and 18O) measurements in semi-arid environments: A soil water balance. *Hydrology and Earth System Sciences*, *20*(2), 715–731. https://doi.org/10.5194/hess-20-715-2016

Gaj, M., & McDonnell, J. J. (2019). Possible soil tension controls on the isotopic equilibrium fractionation factor for evaporation from soil. *Hydrological Processes*, *33*(11), 1629–1634.

Garvelmann, J., Külls, C., & Weiler, M. (2012). A porewater-based stable isotope approach for the investigation of subsurface hydrological processes. *Hydrology and Earth System Sciences*, *16*(2), 631–640.

Gazis, C., & Feng, X. (2004). A stable isotope study of soil water: evidence for mixing and preferential flow paths. *Geoderma*, *119*(1–2), 97–111.

Genssler, H. (1959). *Veranderungen von Boden und Vegetation nach generationsweisem Fichtenanbau*.

Gierke, C., Newton, B. T., & Phillips, F. M. (2016). Soil-water dynamics and tree water uptake in the Sacramento Mountains of New Mexico (USA): a stable isotope study. *Hydrogeology Journal*, *24*(4), 805–818.

Goldsmith, G. R., Allen, S. T., Braun, S., Engbersen, N., González-Quijano, C. R., Kirchner, J. W., & Siegwolf, R. T. W. (2019). Spatial variation in throughfall, soil, and plant water isotopes in a temperate forest. *Ecohydrology*, *12*(2). https://doi.org/10.1002/eco.2059

Goldsmith, G. R., Muñoz-Villers, L. E., Holwerda, F., McDonnell, J. J., Asbjornsen, H., & Dawson, T. E. (2012). Stable isotopes reveal linkages among ecohydrological processes in a seasonally dry tropical montane cloud forest. *Ecohydrology*, *5*(6), 779 –790.

Gootman, K. S., Kellner, E., & Hubbart, J. A. (2020). A comparison and validation of saturated hydraulic conductivity models. *Water*, *12*(7), 2040.

Gralher, B., Herbstritt, B., Weiler, M., Wassenaar, L. I., & Stumpp, C. (2016). Correcting Laser-Based Water Stable Isotope Readings Biased by Carrier Gas Changes. *Environmental Science and Technology*, *50*(13), 7074 –7081. https://doi.org/10.1021/acs.est.6b01124

Hendry, M. J., Schmeling, E., Wassenaar, L. I., Barbour, S. L., & Pratt, D. (2015). Determining the stable isotope composition of pore water from saturated and

unsaturated zone core: Improvements to the direct vapour equilibration laser spectrometry method. *Hydrology and Earth System Sciences*, *19*(11), 4427– 4440. https://doi.org/10.5194/hess-19-4427-2015

Herbstritt, B., Gralher, B., & Weiler, M. F. (2012). Continuous in situ measurements of stable isotopes in liquid water. *Water Resources Research*, *48*(3), 1– 6. https://doi.org/10.1029/2011WR011369

Hervé-Fernández, P., Oyarzún, C., Brumbt, C., Huygens, D., Bodé, S., Verhoest, N. E. C., & Boeckx, P. (2016). Assessing the 'two water worlds' hypothesis and water sources for native and exotic evergreen species in south-central Chile. *Hydrological Processes*, *30*(23), 4227–4241.

Hewlett, J. D. (1982). *Principles of forest hydrology*. University of Georgia press.

Horita, J., Rozanski, K., & Cohen, S. (2008). Isotope effects in the evaporation of water: a status report of the Craig–Gordon model. *Isotopes in Environmental and Health Studies*, *44*(1), 23–49.

Horton, J. H., & Hawkins, R. H. (1965). Flow path of rain from the soil surface to the water table. *Soil Science*, *100*(6), 377–383.

Kelln, C. J., Wassenaar, L. I., & Hendry, M. J. (2001). Stable isotopes (δ18O, δ2H) of pore waters in clay-rich aquitards: A comparison and evaluation of measurement techniques. *Groundwater Monitoring & Remediation*, *21*(2), 108–116.

Kendall, C., & Caldwell, E. A. (1998). Fundamentals of isotope geochemistry. In *Isotope tracers in catchment hydrology* (pp. 51–86). Elsevier.

Majoube, M. (1971). Fractionnement en oxygène 18 et en deutérium entre l'eau et sa vapeur. *Journal de Chimie Physique*, *68*, 1423–1436.

Meißner, M., Köhler, M., Schwendenmann, L., Hölscher, D., & Dyckmans, J. (2014). Soil water uptake by trees using water stable isotopes (δ2H and δ18O)−a method test regarding soil moisture, texture and carbonate. *Plant and Soil*, *376*(1–2), 327–335. https://doi.org/10.1007/s11104-013-1970-z

Mennekes, D., Rinderer, M., Seeger, S., & Orlowski, N. (2021). Ecohydrological travel times derived from in situ stable water isotope measurements in trees during a semi–controlled pot experiment. *Hydrology and Earth System Sciences Discussions*, *February*, 1–34. https://doi.org/10.5194/hess-2020-674

Millar, C., Pratt, D., Schneider, D. J., & McDonnell, J. J. (2018). A comparison of extraction systems for plant water stable isotope analysis. *Rapid Communications in Mass Spectrometry*, *32*(13), 1031–1044. https://doi.org/10.1002/rcm.8136

Mueller, M. H., Alaoui, A., Kuells, C., Leistert, H., Meusburger, K., Stumpp, C., Weiler, M., & Alewell, C. (2014). Tracking water pathways in steep hillslopes by δ18O depth profiles of soil water. *Journal of Hydrology*, *519*, 340–352.

Nemes, A., Wösten, J. H. M., & Lilly, A. (1999). Development of soil hydraulic pedotransfer functions on a European scale: their usefulness in the assessment of soil quality. *Sustainig the Global Farm, Edited by: Stott, DE, Mohtar, RH, and Steinardt, GC, Selected Papers from the 10th International Soil Conservation Organization Meeting Held, 2429*.

Newberry, S. L., Prechsl, U. E., Pace, M., & Kahmen, A. (2017). Tightly bound soil water introduces isotopic memory effects on mobile and extractable soil water pools. *Isotopes in Environmental and Health Studies*, *53*(4), 368–381. https://doi.org/10.1080/10256016.2017.1302446

Nihlgård, B. (1971). Pedological influence of spruce planted on former beech forest soils in Scania, South Sweden. *Oikos*, 302–314.

Oerter, E. J., & Bowen, G. (2017). In situ monitoring of H and O stable isotopes in soil water reveals ecohydrologic dynamics in managed soil systems. *Ecohydrology*, *10*(4), 1–13.

https://doi.org/10.1002/eco.1841
Oerter, E. J., & Bowen, G. J. (2019). Spatio-temporal heterogeneity in soil water stable isotopic composition and its ecohydrologic implications in semiarid ecosystems. *Hydrological Processes*, *33*(12), 1724–1738. https://doi.org/10.1002/hyp.13434
Oldenburg, U. (2008). *Skript Bodenpraktikum*.
Orlowski, N., & Breuer, L. (2020). Sampling soil water along the pF curve for δ2H and δ18O analysis. *Hydrological Processes*, *34*(25), 4959–4972. https://doi.org/10.1002/hyp.13916
Orlowski, N., Breuer, L., & Mcdonnell, J. J. (2016). Critical issues with cryogenic extraction of soil water for stable isotope analysis. *Ecohydrology*, *9*(1), 3–10. https://doi.org/10.1002/eco.1722
Orlowski, N., Pratt, D. L., & McDonnell, J. J. (2019). Intercomparison of soil pore water extraction methods for stable isotope analysis and interpretation of hillslope runoff sources. *Hydrological Processes*, *33*(22), 2939–2954. https://doi.org/10.1002/hyp.13539
Rothfuss, Y., Vereecken, H., & Brüggemann, N. (2013). Monitoring water stable isotopic composition in soils using gas-permeable tubing and infrared laser absorption spectroscopy. *Water Resources Research*, *49*(6), 3747–3755.
Schmid, I. (2002). The influence of soil type and interspecific competition on the fine root system of Norway spruce and European beech. *Basic and Applied Ecology*, *3*(4), 339–346.
Schume, H., Jost, G., & Hager, H. (2004). Soil water depletion and recharge patterns in mixed and pure forest stands of European beech and Norway spruce. *Journal of Hydrology*, *289*(1–4), 258–274. https://doi.org/10.1016/j.jhydrol.2003.11.036
Seeger, S., & Weiler, M. (2021). Temporal dynamics of tree xylem water isotopes: In situ monitoring and modeling. *Biogeosciences*, *18*(15), 4603–4627. https://doi.org/10.5194/bg-18-4603-2021
Seki, K. (2007). SWRC fit–a nonlinear fitting program with a water retention curve for soils having unimodal and bimodal pore structure. *Hydrology and Earth System Sciences Discussions*, *4*(1), 407–437.
Solutions, T. E. S. (2017). *压力传感器力Pressure Transducer*. 15–15.
Sprenger, M., & Allen, S. T. (2020). What Ecohydrologic Separation Is and Where We Can Go With It. In *Water Resources Research* (Vol. 56, Issue 7). Blackwell Publishing Ltd. https://doi.org/10.1029/2020WR027238
Sprenger, M., Leistert, H., Gimbel, K., & Weiler, M. (2016). Illuminating hydrological processes at the soil-vegetation-atmosphere interface with water stable isotopes. In *Reviews of Geophysics* (Vol. 54, Issue 3, pp. 674–704). Blackwell Publishing Ltd. https://doi.org/10.1002/2015RG000515
Sprenger, M., Llorens, P., Cayuela, C., Gallart, F., & Latron, J. (2019). Mechanisms of consistently disjunct soil water pools over (pore) space and time. *Hydrology and Earth System Sciences*, *23*(6), 2751–2762.
Sprenger, M., Seeger, S., Blume, T., & Weiler, M. (2016). Travel times in the vadose zone: Variability in space and time. *Water Resources Research*, *52*(8), 5727–5754. https://doi.org/10.1002/2015WR018077
Sprenger, M., Tetzlaff, D., Buttle, J., Carey, S. K., McNamara, J. P., Laudon, H., Shatilla, N. J., & Soulsby, C. (2018). Storage, mixing, and fluxes of water in the critical zone across northern environments inferred by stable isotopes of soil water. *Hydrological Processes*, *32*(12), 1720–1737. https://doi.org/10.1002/hyp.13135
Tomasella, J., & Hodnett, M. G. (1996). Soil hydraulic properties and van Genuchten parameters for an oxisol under pasture in central Amazonia. *Amazonian Deforestation and Climate*.

Van der Straaten, C. M., & Mook, W. G. (1983). Stable isotopic composition of precipitation and climatic variability. *Palaeoclimates and Palaeowaters: A Collection of Environmental Isotope Studies*, 53–64.

Van Genuchten, M. T. (1980). A closed-form equation for predicting the hydraulic conductivity of unsaturated soils. *Soil Science Society of America Journal*, *44*(5), 892–898.

Volkmann, T. H. M., & Weiler, M. (2014). Continual in situ monitoring of pore water stable isotopes in the subsurface. *Hydrology and Earth System Sciences*, *18*(5), 1819–1833. https://doi.org/10.5194/hess-18-1819-2014

Wassenaar, L. I., Hendry, M. J., Chostner, V. L., & Lis, G. P. (2008a). High resolution pore water δ2H and δ18O measurements by H2O(liquid)-H2O (vapor) equilibration laser spectroscopy. *Environmental Science and Technology*, *42*(24), 9262–9267. https://doi.org/10.1021/es802065s

Wassenaar, L. I., Hendry, M. J., Chostner, V. L., & Lis, G. P. (2008b). High resolution pore water δ2H and δ18O measurements by H2O(liquid)-H2O (vapor) equilibration laser spectroscopy. *Environmental Science and Technology*, *42*(24), 9262–9267. https://doi.org/10.1021/es802065s

Yang, R., & Xing, B. (2021). A comparison of the performance of different interpolation methods in replicating rainfall magnitudes under different climatic conditions in chongqing province (China). *Atmosphere*, *12*(10). https://doi.org/10.3390/atmos12101318

Zhao, L., Wang, L., Cernusak, L. A., Liu, X., Xiao, H., Zhou, M., & Zhang, S. (2016). Significant difference in hydrogen isotope composition between xylem and tissue water in Populus euphratica. *Plant, Cell & Environment*, *39*(8), 1848–1857.

List of Abbreviations

Name	Unit	Acronym
Analysis of variances		ANOVA
Cation exchange capacity		CEC
Carbon to nitrogen ratio		C/N
Cavity ring down spectroscopy		CRDS
Electronic conductivity	[µS cm^{-1}]	EC
Potential evaporation	[mm day^{-1}]	ET_0
Fluorinated ethylene propylene		FEP
Generalized linear model		GLM
Global meteoric water line		GMWL
Deuterium		^{2}H
Leaf area index	[-]	LAI
Local meteoric water line	[-]	LMWL
Matric potential	[hPa]	MP
Oxygen-18		^{18}O
Polyethylene		PE
Photosynthetic active radiation	[µmol m^{-2} s^{-1}]	PAR
Potential of hydrogen	$\log_{10}$ [H^{+}]	pH
Root square error		RSE
Soil-plant-atmosphere-continuum		SPAC
polyvinyl chloride		PVC
Soil water retention curve		SWRC
Soil water content	[Vol.%]	θ
Vapor pressure deficit	[kPa]	VPD
Volumetric water content	[Vol.%]	VWC
Water isotope probe		WIP

Appendix

List of Figures Appendix

List of Tables Appendix

Table A. 1: Average volumetric water content values grouped by stand and soil depth

			[Vol.%]			
Soil Depth [cm]	**Beech variability**	**Spruce variability**	**Mixed variability**	**Beech average**	**Spruce average**	**Mixed average**
5	13.69 – 26.7	14.72 -28.74	13.55 – 26.25	20.20	21.73	19.90
20	12.57 – 24.04	16.09 – 29.64	11.69 – 21.08	18.30	22.86	16.38
40	15.50 – 27.97	18.94 – 41.50	18.33 – 27.97	21.73	30.22	23.15
90	26.13 – 36.19	27.32 – 45.11	10.95 -16.31	31.16	36.21	13.63

Table A. 2: Fitted van Genuchten parameters for soil water retention characteristics for plot A,C,E,F,H,I at 20 cm soil depth

Soil type	θ_{sat} **[m³ m^{-3}]**	θ_{res} **[m³ m^{-3}]**	**n [-]**	α **[m^{-1}]**
Clay loam	0.44	0.100	1.7714	0.024076
Silty loam	0.41	0.035	1.2531	0.018512
Sandy loam	0.40	0.080	4.5710	0.020766
A (20cm)	0.29	0.022	0.7676	0.062608
C (20cm)	0.17	0.004	1.3130	0.037088
E (20cm)	0.21	0.814	1.6699	0.021612
F (20cm)	0.24	0.144	1.6075	0.030162
J (20cm)	0.14	0.001	1.1903	0.011037
I (20cm)	0.22	0.100	1.7438	0.068302

Table A. 3: Isotope values equilibration bag method 07.16.2021

Plot	**δ^2H [‰]**	**SD[±]**	**δ^{18}O[‰]**	**SD[±]**
A	-46.33	0.84	-6.96	0.21
B	-51.49	0.71	-7.09	0.20
C	-52.90	0.69	-7.55	0.2
D	-53.93	0.69	-7.64	0.2
E	-49.01	0.74	-6.28	0.21
F	-50.56	0.77	-6.87	0.23
G	-48.46	0.62	-6.32	0.21
H	-47.86	0.72	-6.35	0.21
I	-45.78	0.71	-6.17	0.22

Table A. 4: Isotope values equilibration bag method 08.17.2021

Plot	$\delta^{2}H$ [‰]	SD[±]	$\delta^{18}O$[‰]	SD[±]
A	-56.75	0.79	-7.66	0.20
B	-51.75	0.69	-7.22	0.21
C	-49.99	0.68	-6.99	0.21
D	-53.35	0.68	-7.40	0.21
E	-59.68	0.83	-8.23	0.24
F	-53.21	0.76	-7.32	0.21
G	-52.51	0.76	-6.98	0.24
H	-53.01	0.78	-6.88	0.24
I	-54.98	0.69	-7.58	0.21

Table A. 5: Isotope values equilibration bag method 10.05.2021

Plot	$\delta^{2}H$ [‰]	SD[±]	$\delta^{18}O$[‰]	SD[±]
A	-50.90	0.75	-6.66	0.22
B	-47.29	0.76	-6.17	0.19
C	-52.02	0.75	-6.86	0.22
D	-51.19	0.66	-6.94	0.23
E	-57.43	0.75	-6.97	0.22
F	-55.87	0.76	-7.29	0.23
G	-52.42	0.73	-6.16	0.21
H	-55.56	0.63	-6.73	0.20
I	-58.87	0.73	-7.54	0.21

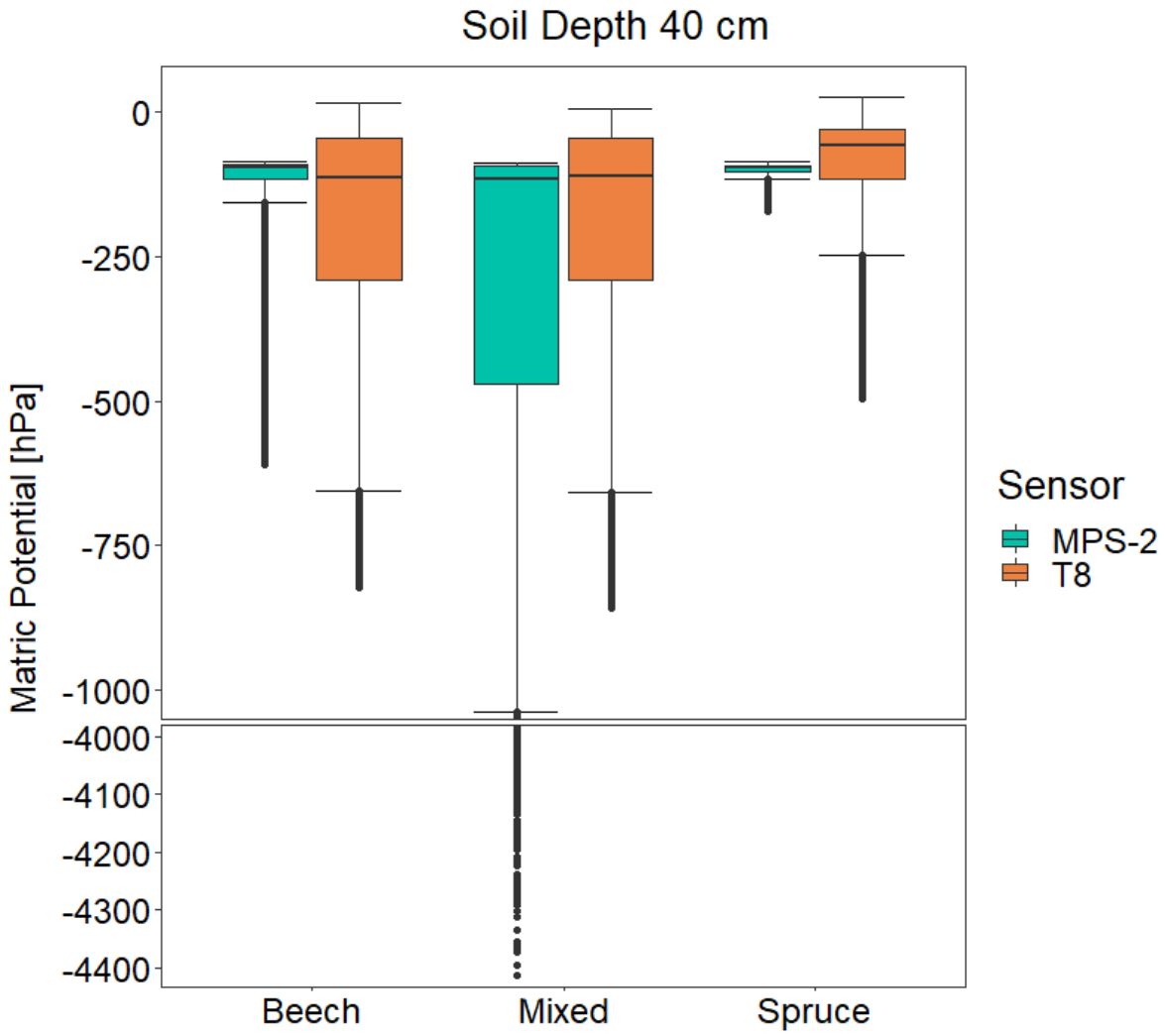

Figure A. 1: performance comparison of MPS-2 and T8 Sensors (at 40 cm soil depth)

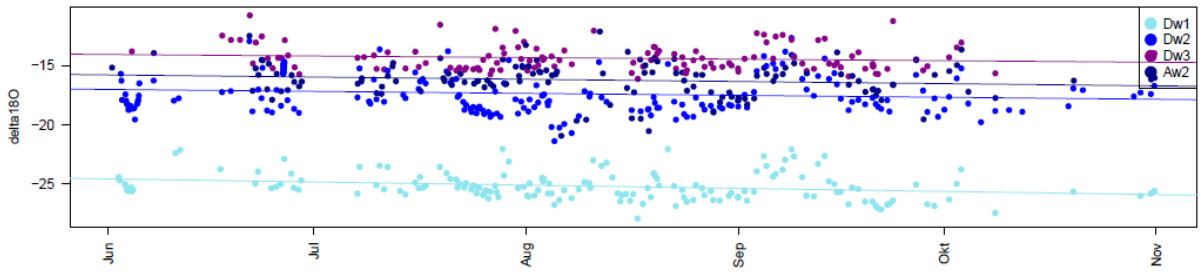

Figure A. 2: Liquid vapor correction: Measured $\delta^{18}O$ values of water vapor from standard waters

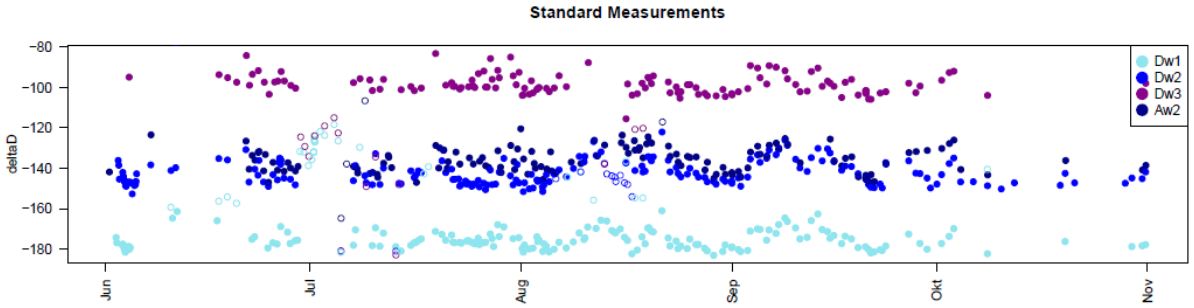

Figure A. 3: Liquid vapor correction: Measured δ^2H values of water vapor from standard waters

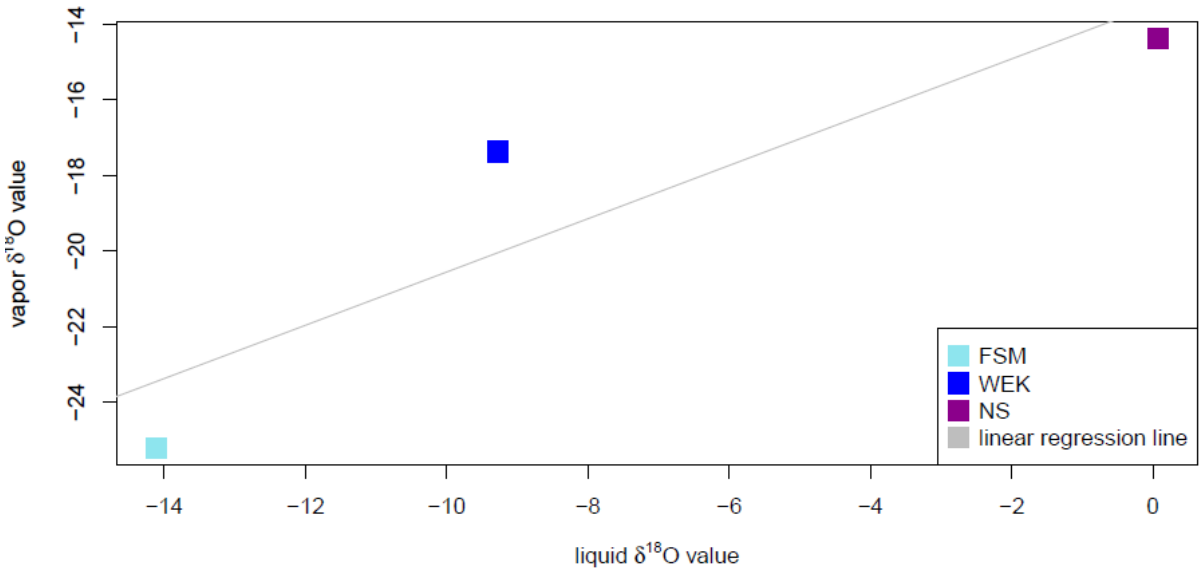

Figure A. 4: Liquid vapor correction: Linear regression of vapor and liquid $\delta^{18}O$ values (R^2=0.64)

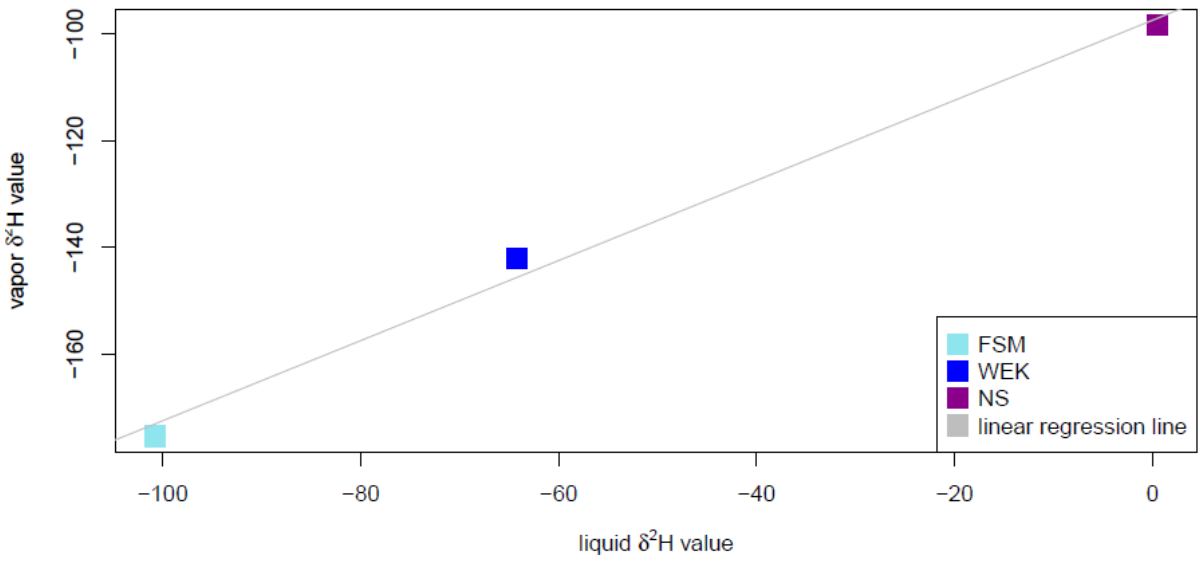

Figure A. 5: Liquid vapor correction: Linear regression of vapor and liquid δ^2H values (R^2=0.99)

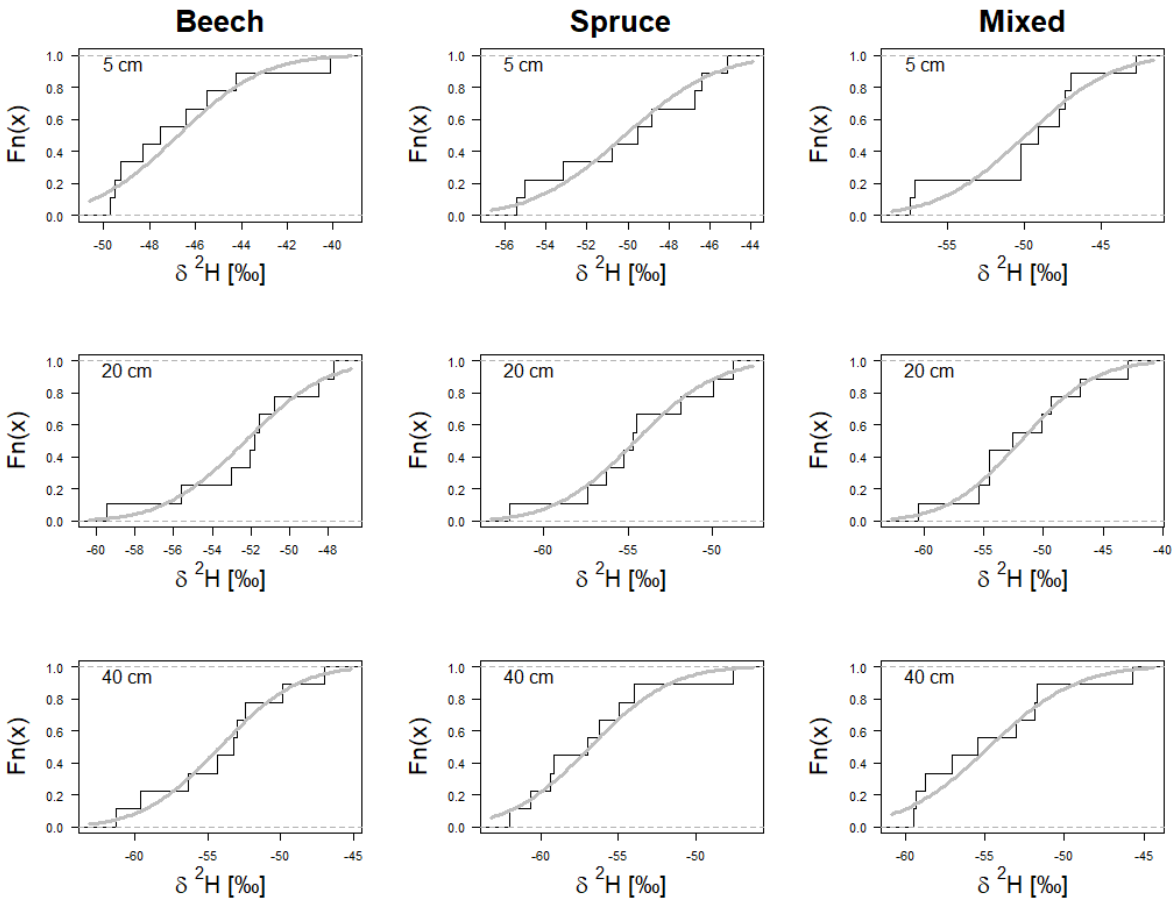

Figure A. 6: cumulative distribution function of δ^2H values at each plot and soil depth respectively. Values originate from all three the equilibration bag method samplings

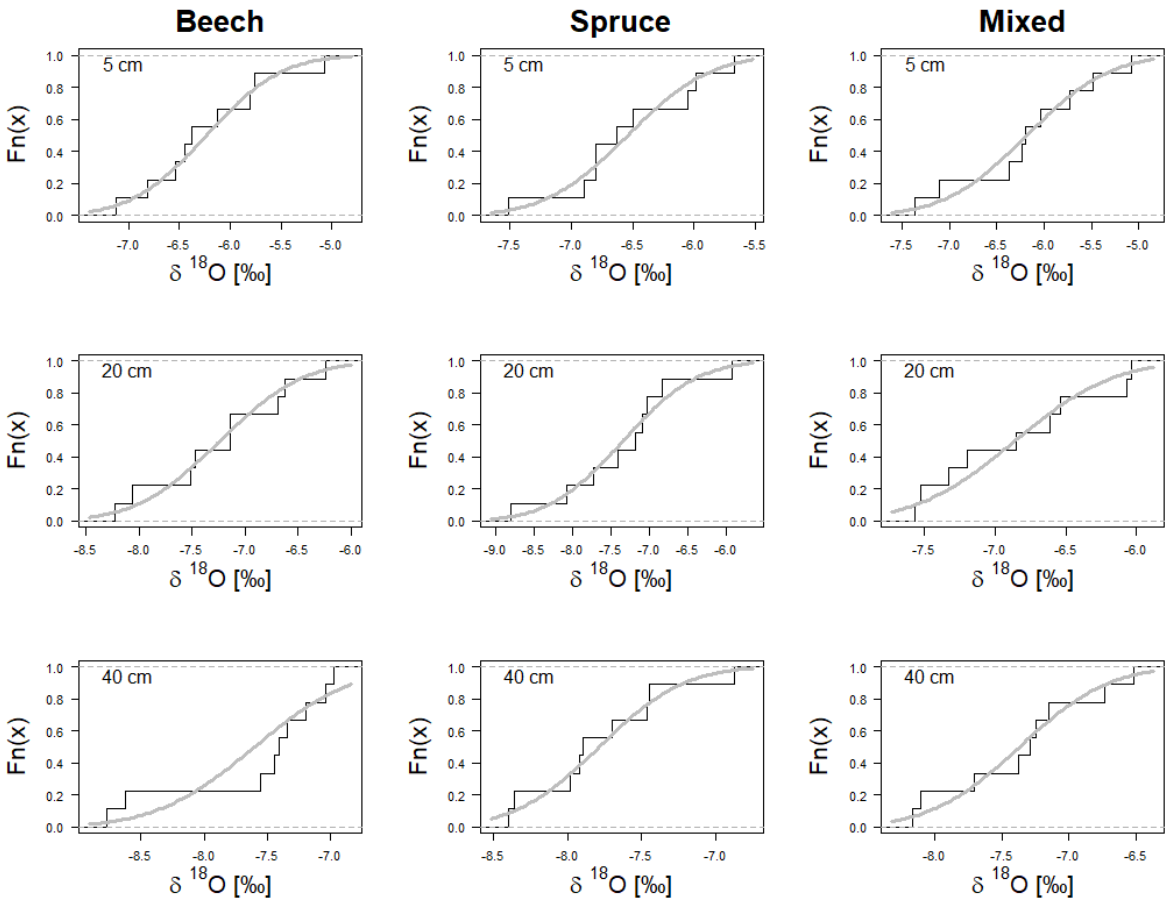

Figure A. 7: cumulative distribution function of $\delta^{18}O$ values at each plot and soil depth respectively. Values originate from all three the equilibration bag method samplings

Table A. 6: Distribution of $\delta^{2}H$ values and results of Anderson Darling test for normal distribution (equilibration bag method)

Stand	Soil depth	p- value	mean	sd	median
Beech	5	0.815	-46.74	3.11	-47.52
	20	0.886	-52.27	3.55	-51.81
	40	0.154	-54.14	4.47	-53.24
Spruce	5	0.934	-50.13	3.78	-49.53
	20	0.984	-54.53	4.02	-54.72
	40	0.065	-56.77	4.36	-56.96
Mixed	5	0.722	-49.86	4.75	-49.06
	20	0.993	-51.89	5.19	-52.58
	40	0.086	-54.69	4.56	-55.46

Table A. 7: Distribution of $\delta^{18}O$ values and results of Anderson Darling test for normal distribution (equilibration bag method)

Stand	Soil depth	p- value	mean	sd	median
Beech	5	0.991	-6.23	0.62	-6.38
	20	0.982	-7.23	0.66	-7.14
	40	0.409	-7.6	0.65	-7.41
Spruce	5	0.952	-6.54	0.56	-6.63
	20	0.979	-7.33	0.81	-7.17
	40	0.961	-7.78	0.48	-7.89
Mixed	5	0.973	-6.18	0.72	-6.2
	20	0.896	-6.86	0.59	-6.85
	40	0.961	-7.36	0.55	-7.29

Table A. 8: Variance analysis of $\delta^{2}H$ values of "Group by stand" (equilibration bag method)

Group	Soil depth	p- value	Levene's Test
Beech/Spruce/Mixed	5	0.107	0.654
Beech/Spruce		0.183	
Beech/Mixed		0.233	
Spruce/Mixed		0.988	
Beech/Spruce/Mixed	20	0.854	0.479
Beech/Spruce		0.518	
Beech/Mixed		0.980	
Spruce/Mixed		0.409	
Beech/Spruce/Mixed	40	0.797	0.949
Beech/Spruce		0.437	
Beech/Mixed		0.962	
Spruce/Mixed		0.593	

Table A. 9: Variance analysis of $\delta^{18}O$ values of "Group by stand" (equilibration bag method)

Group	Soil depth	p- value	Levene's Test
Beech/Spruce/Mixed	5	0.867	0.866
Beech/Spruce		0.571	
Beech/Mixed		0.984	
Spruce/Mixed		0.468	
Beech/Spruce/Mixed	20	0.265	0.908
Beech/Spruce		0.947	
Beech/Mixed		0.498	
Spruce/Mixed		0.329	
Beech/Spruce/Mixed	40	0.397	0.921
Beech/Spruce		0.771	
Beech/Mixed		0.661	
Spruce/Mixed		0.280	

Table A. 10: Variance analysis of $\delta^{2}H$ values of "Group by soil" (equilibration bag method)

		t-test	
Group	**Soil depth**	**p- value**	**Levene's Test**
Clay loam/	5	0.135	0.654
Silt loam	20	0.634	
	40	0.654	

Table A. 11: Variance analysis of $\delta^{18}O$ values of "Group by soil" (equilibration bag method)

		t-test	
Group	**Soil depth**	**p- value**	**Levene's Test**
Clay loam/	5	0.927	0.947
Silt loam	20	0.767	
	40	0.702	

Table A. 12: GLM with all predictors included

		GLM	
Dependend variable	**Independend variable**	**p- value**	**Adj. R^2**
δ^2H	P, Tsoil, VWC, C/N, CEC, pH	2.2e-16 ***	0.32
	P	1.9e-06 ***	
	Tsoil	2.5e-11 ***	
	VWC	0.14	
	C/N	3.3e-06 ***	
	pH	4.9e-03 ***	
	Al	0.42	
	Ca	0.19	
	Fe	0.07	
	Mg	0.35	
	K	0.16	
	Mn	0.11	
	Na	0.16	

Signif. codes: 0 '***' 0.001 '**' 0.01 '*' 0.05 '.' 0.1 ' ' 1

Table A. 13: GLM results with excluded predictor C/N

		GLM	
Dependend variable	**Independend variable**	**p- value**	**Adj. R^2**
δ^2H	P, Tsoil, VWC, CEC, pH	2.2e-16 ***	0.28
	P	5.3e-06 ***	
	Tsoil	1.1e-09 ***	
	VWC	0.79	
	pH	1.8e-05 ***	
	Al	0.23	
	Ca	9.2e-03 ***	
	Fe	0.27	
	Mg	3.8e-03 **	
	K	9.9e-03 **	
	Mn	0.25	
	Na	0.40	

Signif. codes: 0 '***' 0.001 '**' 0.01 '*' 0.05 '.' 0.1 ' ' 1

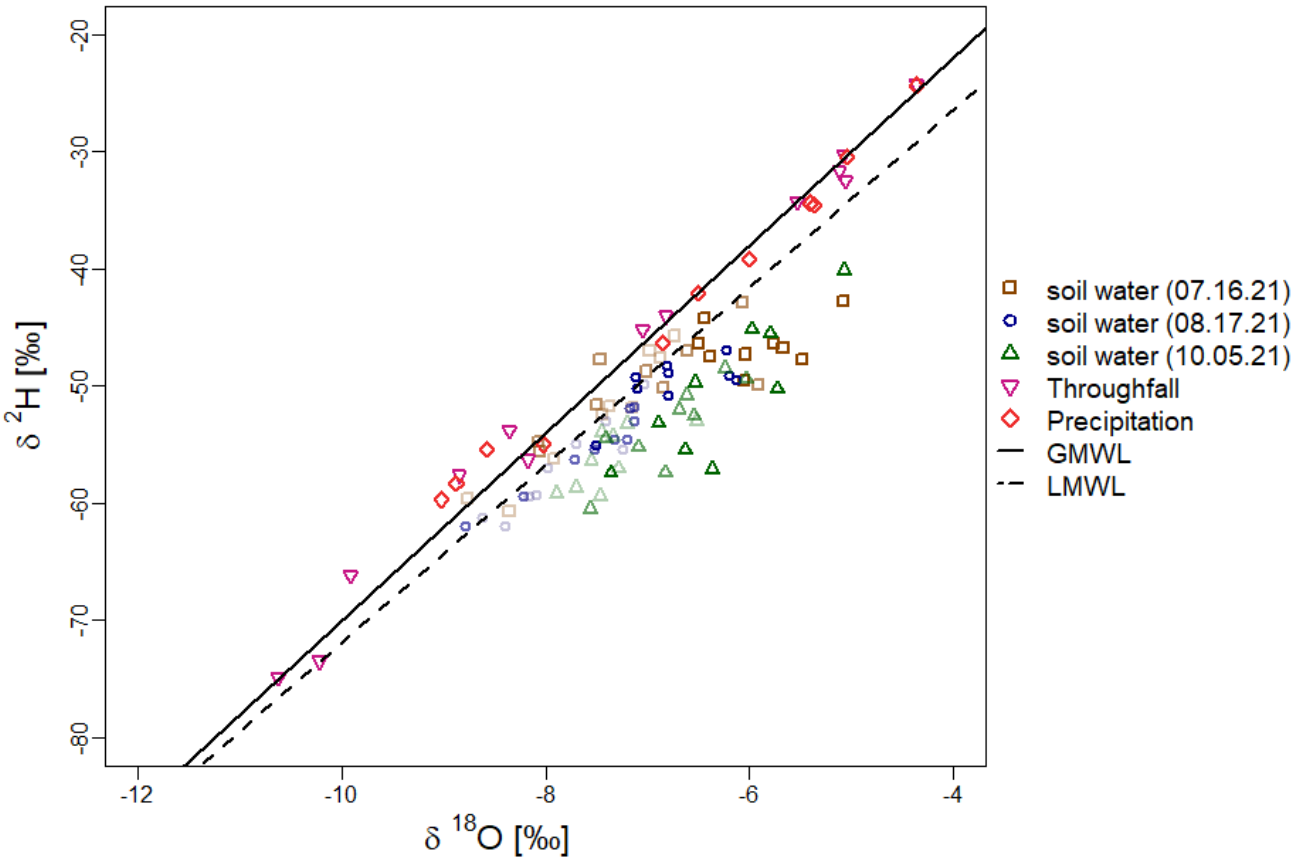

Figure A. 8: Dual isotope plot of values from soil water from equilibration bag method, precipitation and throughfall. In addition, GMWL and LMWL for orientation

Table A. 14: GLM results with dummy variable date

GLM			
Dependend variable	**Independend variable**	**p- value**	**Adj. R^2**
δ^2H	P, Tsoil, VWC, C/N, CEC, pH, Date	2.2e-16 ***	0.59
	P	0.43	
	Tsoil	0.25	
	VWC	2.5e-03 ***	
	C/N	0.16	
	pH	4.2e-11 ***	
	Al	0.50	
	Ca	0.82	
	Fe	0.67	
	Mg	0.15	
	K	0.84	
	Mn	0.25	
	Na	0.007 **	
	Date (dummy)	5.3e-07 ***	

Signif. codes: 0 '***' 0.001 '**' 0.01 '*' 0.05 '.' 0.1 ' ' 1

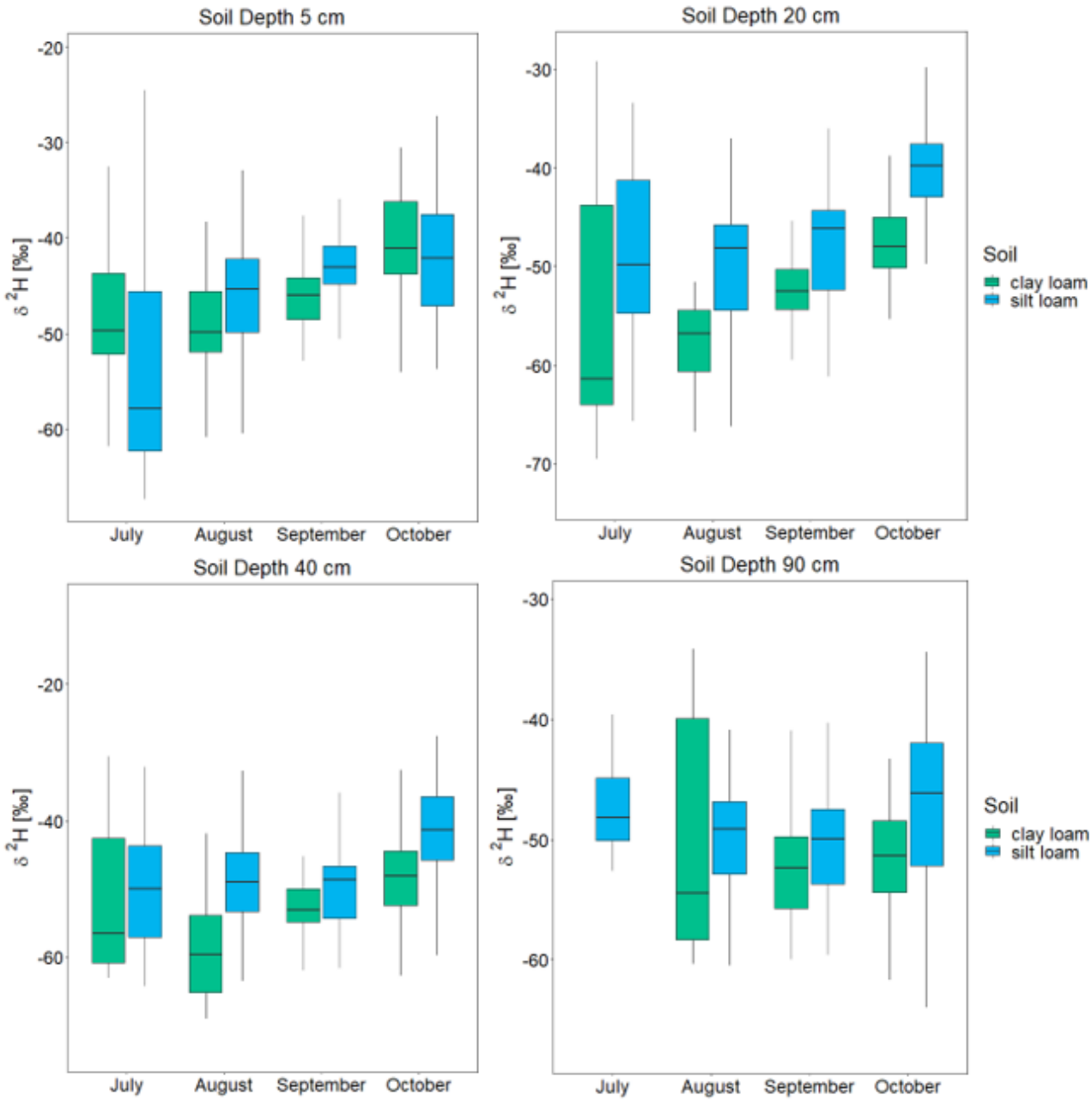

Figure A. 9: Boxplots of spatiotemporal soil water δ^2H values from in situ measurements separated by soil type and differentiable by color

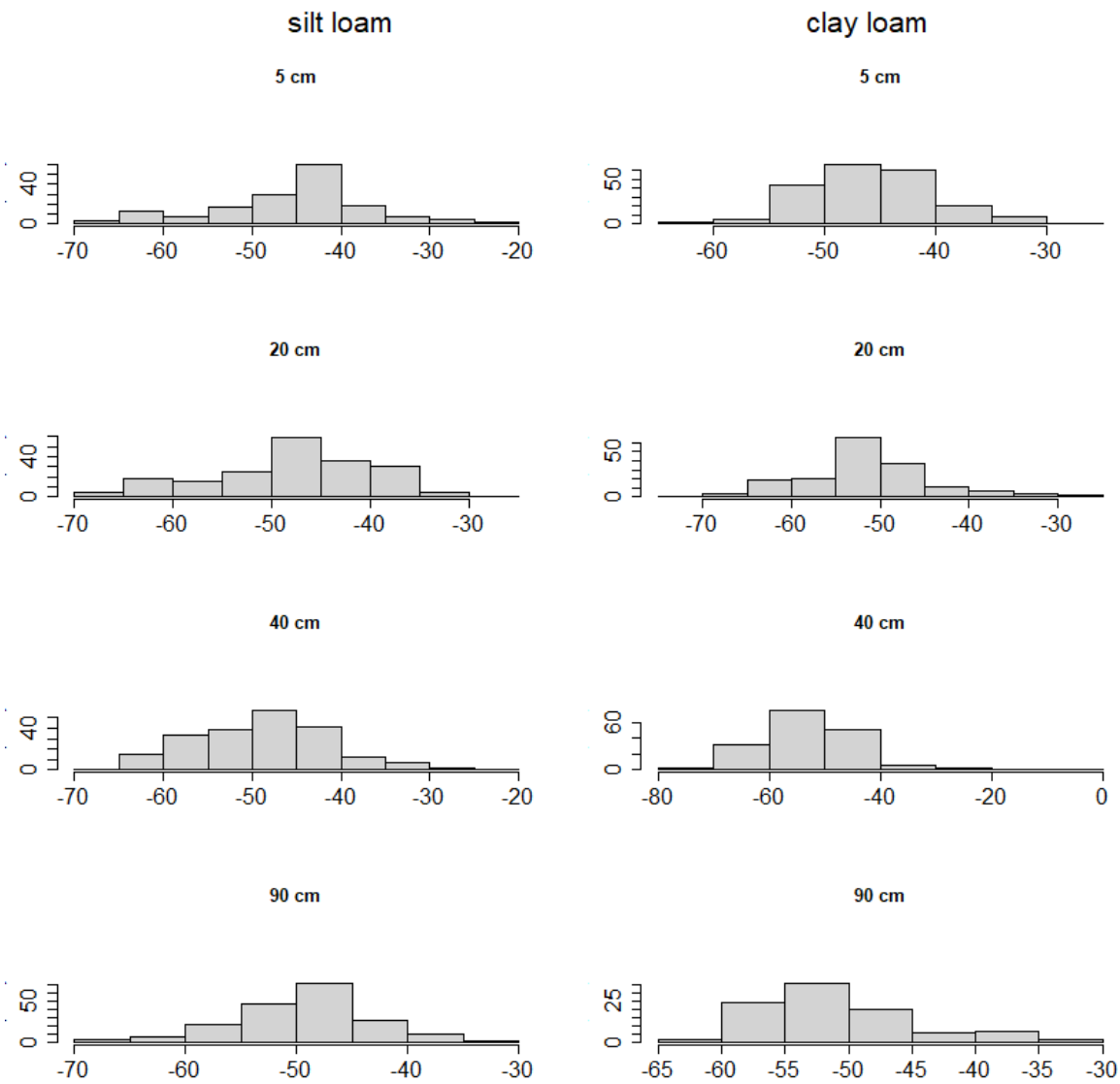

Figure A. 10: Distribution histograms of soil water δ^2H values of the two subgroups of "Group by Soil"

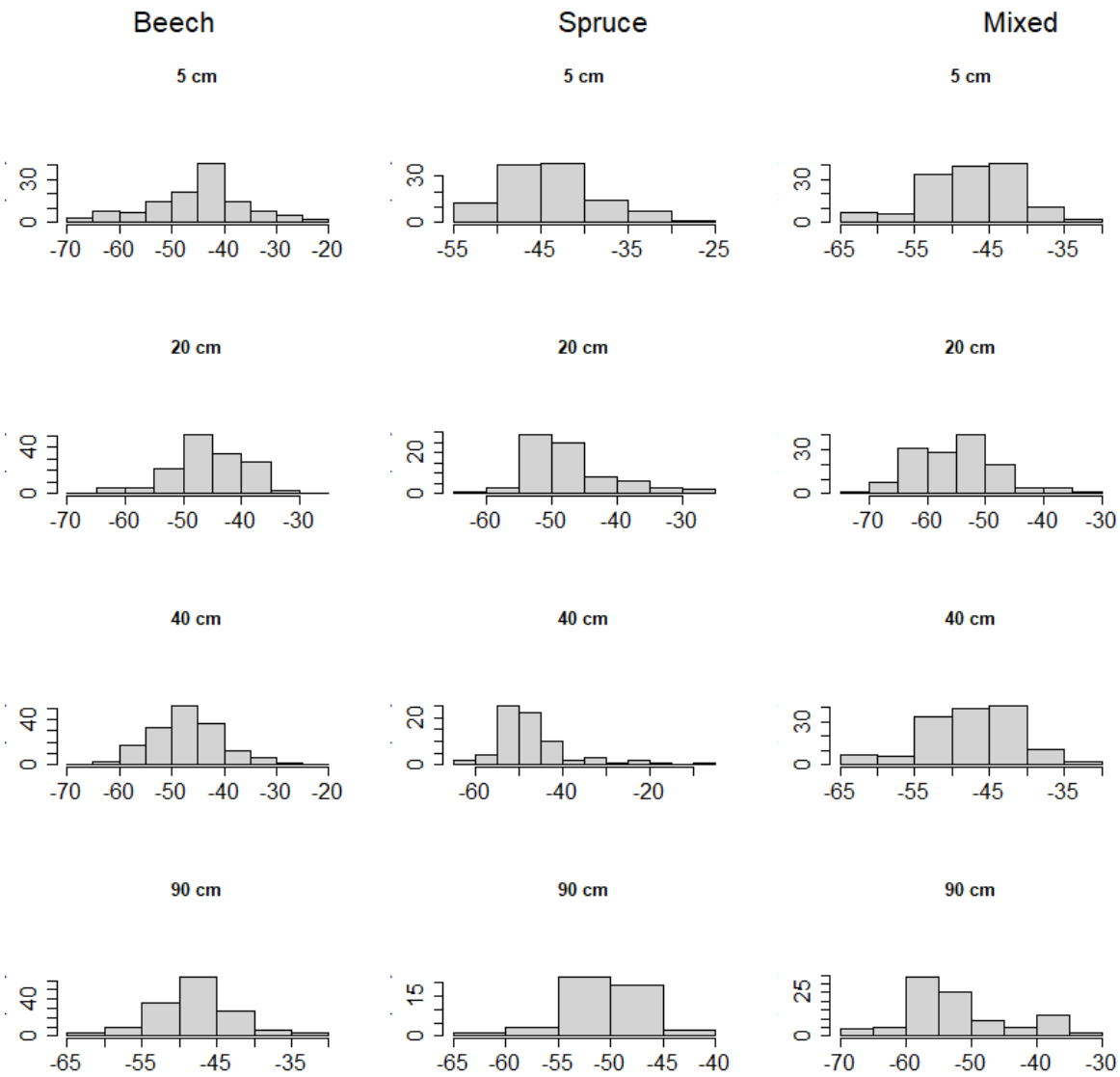

Figure A. 11: Figure A. 10: Distribution histograms of soil water δ²H values of the three subgroups of "Group by Stand"

Declaration

I hereby declare that I have prepared this thesis independently and only with the help of the indicated aids.

Place, date Signature